LANGMUIR

Article

pubs.acs.org/Langmuir

Molecular Simulation Study of the Early Stages of Formation of Bioinspired Mesoporous Silica Materials

Alessia Centi and Miguel Jorge*

Department of Chemical and Process Engineering, University of Strathclyde, James Weir Building, 75 Montrose Street, Glasgow G1 1XJ, United Kingdom of Great Britain and Northern Ireland

Supporting Information

ABSTRACT: The use of bioinspired templates, such as polyamines and polypeptides, could lead to significant improvements in the synthesis conditions under which mesoporous materials are traditionally produced, removing the need for strong pH as well as high temperature or pressure. In this work, we perform atomistic molecular dynamics simulations of 1,12-diaminododecane surfactants, in water and in the presence of silica monomers, to investigate the early stages of synthesis of one of the first examples of bioinspired silica materials. Different surfactant concentrations and pH were considered, clarifying the influence of the charge state of the molecules on the self-assembly process. We show that the amphiphilic amines form stable lamellar structures at equilibrium in the range from intermediate to high pH values. In a later stage, when silica species are added to the system, our results reveal that, in the same range of pH, silicates strongly adsorb around these aggregates at the interface with water. This causes a considerable modification of the curvature of the layer, which suggests a tendency for the system to evolve from a lamellar phase to the formation of vesicle structures. Furthermore, we show that silica monomers are able to penetrate the layer spontaneously when defects are created as a result of surfactants' head-to-head repulsion. These findings are in agreement with experimental observations and support the pillaring mechanism postulated for this class of materials. However, our simulations indicate that the aggregation process is driven by charge matching between surfactant heads and silica monomers rather than by hydrogen bond interactions between neutral species, as had been previously hypothesized.

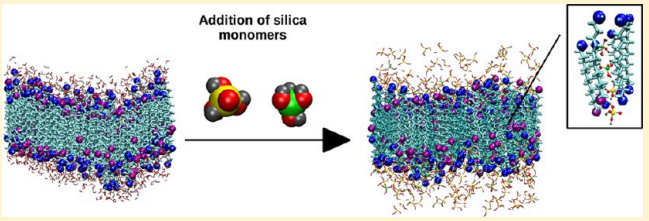

1. INTRODUCTION

Silica-based porous materials are used in a wide range of applications such as catalysis, separation processes, drug delivery, and so forth because of their remarkable features: large surface areas, high pore volumes, and potential for functionalization. Although industrial silica is usually produced under harsh conditions (high temperature and pressure, strongly acidic or alkaline media), nature seems to have found a better way to produce hierarchically ordered silica structures, with dimensions ranging from tens of nanometers up to hundreds of micrometers.[1] Such morphological control is hardly reached in industrially produced silica and never under mild conditions (aqueous media, ambient temperature, neutral pH). Biological systems, such as diatoms, sponges, and radiolarians, for example, form their sophisticated skeletons and shells by transferring silicic acid from marine environments and incorporating it intra- or extracellularly to produce ornate amorphous silica structures.[2] This very common but complex process, denoted as biosilicification, has attracted increasing interest in recent years, directed at capturing the mechanism of silica synthesis under such mild conditions and possibly mimicking it for the production of bioinspired silica-based materials.[3] Several phenomenological models have been proposed in order to explain experimental observations, but a complete understanding of the synthesis mechanisms at the molecular level is still lacking. Such knowledge is essential to providing further control over the properties of the solids and enabling the targeted design of bioinspired mesoporous silica materials.

In previous studies, specific polypeptides and proteins called silaffins[4,5] and silicateins[6] have been extracted from diatoms and sponges, respectively. Furthermore, long-chain polyamines have been discovered in both species, but more interestingly, polyamines are the only type of biomolecules found in a particular order of diatoms called *Coscinodiscus*,[7] which exhibit hexagonal arrays that are reminiscent of the cylindrical pore structures observed in periodic mesoporous silicas.[8] Here we will focus our attention on the role of polyamines as templates for silica precipitation.

To our knowledge, the first attempt to rationalize the honeycomb-like structure observed in diatoms belonging to the genus of *Coscinodiscus* was in 2002 when Sumper[7] proposed a mechanistic model based on repeating phase separation processes in which emulsions of microdroplets containing polyamines are gradually reduced to aggregates of lower size (i.e., nanodroplets and micelles) while arranging in a hexagonal

Received: May 6, 2016
Revised: June 16, 2016
Published: June 24, 2016

DOI: 10.1021/acs.langmuir.6b01731
Langmuir 2016, 32, 7228−7240

fashion. Silica is speculated to precipitate at the interface, where the droplets are in contact with an aqueous environment rich in silicic acid, causing their breakage into smaller units due to polyamine coprecipitation. The process keeps repeating until the complete depletion of amine sources, causing phase separation to stop. Even though this model is able to qualitatively explain patterns and structures observed in nature, alternative models have been proposed in this context. In fact, just a few years later, in 2005, Vrieling et al.[9] suggested that the largest aggregates are not formed at the beginning of the process but toward the end. In Vrieling's model, it is the presence of silaffins and polyamines that is considered to cause silica to form aggregates of increasing size. This example illustrates the many uncertainties that still need to be clarified to fully understand biosilicification, particularly concerning the role played by polyamine surfactants, silicic acid, ions, and their reciprocal interactions at the molecular level.

As well as studying the morphogenesis of cell walls and structures observed in marine organisms, scientists have also looked at biosilicification as an inspiring process for mimicking the production of porous materials in a more efficient way. One of the first examples of a biomimetic templating approach applied to the design of porous silica materials was reported by Tanev and Pinnavaia.[10] Diamines with variable-length alkyl chains (from 8 to 12 carbons) were used as templating agents for silica precipitation from tetraethyl orthosilicate (TEOS) aqueous solutions. Synthesis occurs at ambient temperature, and the product obtained, denoted as MSU-V, shows a hierarchical multilamellar structure. This structure is proposed to arise from interpenetrating vesicles of elliptical shape containing densely packed diamine surfactants (sizes range from 300 to 600 nm when C12 surfactants are used[11]), alternated with layers consisting of water and silica species. Silica pillars run perpendicular to these layers and connect the inorganic (silica) regions while affording morphologies that resemble biomineralization. Tanev and Pinnavaia[10] postulated a cooperative mechanism of formation for these materials based on a hydrophilic−hydrophobic balance and hydrogen-bonding interactions between neutral diamines and neutral silica species in solution. According to their hypothesis, hydrophilic−hydrophobic interactions are responsible for the formation of lamellar aggregates and the consequent curvature of the interface that leads to the formation of vesicles. Hydrogen bonds between silicates and surfactant headgroups participate in this process while promoting silica oligomer growth in both horizontal (layers) and vertical (pillars) directions as a result of the transfer of some silicates across the vesicular interface. To our knowledge, no further studies, theoretical or experimental, have attempted to validate or disprove this proposed mechanism.

In the context of templated mesoporous materials synthesis, simulation techniques have proven to be a powerful tool to complement experimental studies in the investigation of formation mechanisms, often providing the link between microscopic phenomena and macroscopic observations.[12] One avenue, pioneered by Siperstein and Gubbins[13] and later extended by Monson and co-workers,[14] makes use of coarse-grained lattice models. These were able to clarify many aspects of the synthesis mechanism of mesoporous silica but rely on several simplifying assumptions regarding interactions between molecules in the synthesis solution. In more recent years, the increase in computer capabilities allowed for more detailed atomistic simulations in which all of the species taking part in the synthesis process are modeled explicitly. Jorge and co-workers[15−17] performed large molecular dynamics simulations of *n*-decyltrimethylammonium bromide (DeTAB) surfactants in the absence and presence of silica monomers and oligomers in order to study the self-assembly process that leads to the formation of periodic mesoporous silica materials. It was found that the strong interactions between surfactant headgroups and silicates are responsible for the adsorption of these species at the interface and the subsequent micellar growth while promoting reciprocal interactions among these aggregates.[16,17] Computer resources are the bottleneck in atomistic modeling; therefore, to be able to obtain a representative picture of this system at later stages of synthesis, the same group developed a coarse-grained approach based on the MARTINI model,[18,19] which demonstrated that the driving force for the sphere-to-rod transition in periodic mesoporous silica (PMS) materials synthesis is the presence of anionic silicates,[20] and that oligomers are necessary to induce micellar aggregation and the cooperative formation of hexagonally ordered silica materials.[21]

In the present work, the formation mechanism of bioinspired silica materials is investigated at the molecular level by means of atomistic molecular dynamics simulations. This technique is applied to study the precursor solution of MSU-V materials,[10,11] with an approach similar to that used previously to study the synthesis of MCM-type materials[17] in order to provide a detailed analysis of the interactions between silicates and surfactants. We present results from simulations at different concentrations and pH showing that neutral and singly charged polyamine surfactants form ordered lamellar phases, whereas doubly charged surfactants on their own do not produce similar aggregates. In the last part of our work, we added silicic acid monomers to the system, showing how they interact with polyamine molecular aggregates and influence their structure. The article is organized as follows: in section 2, we describe the computational methods and system preparation; the reference solution (without silica) is described in sections 3.1 and 3.2; and the monomeric solution is discussed in section 3.3. In section 3.4, we describe the results from simulations at the pH representing conditions close to those used experimentally, and finally in section 4, we present our conclusions.

2. COMPUTATIONAL METHODS

To investigate the formation mechanism of bioinspired silica materials, we considered a solution of 1,12-diaminododecane (DADD) and a monomeric silica source at several pH values. Our experimental benchmark is the work of Tanev and Pinnavaia[10,11] which describes the synthesis of MSU-V materials with a relatively simple biomimetic approach. Their reacting mixture is composed of a solution of DADD in ethanol and water to which TEOS is added in the proportion 0.26 DADD/13.1 ethanol/50.8 water/1 TEOS. In our MD simulations, we have chosen to study a simplified system for computational expediency. First, we neglect ethanol and replace it with water because we do not expect it to play an important role during structure formation. We also use a lower silica to amine ratio (1:1 or 2:1 instead of approximately 4:1) to facilitate comparison between different solutions on a equal basis, as explained in more detail later.

Three main types of simulations were performed: (a) the reference solution, containing only DADD and water (sections 3.1 and 3.2); (b) the monomeric solution, which also included silica monomers to represent the early stage of formation of MSU-V materials (section 3.3); and (c) a system representing conditions close to those in the experiment (section 3.4). Most simulations started from a random distribution of all species in the simulation box, but for several cases, we also performed simulations starting from preformed surfactant

DOI: 10.1021/acs.langmuir.6b01731
Langmuir 2016, 32, 7228−7240

Table 1. Simulation Characteristics

	name	length	no. of surfactant molecules	no. of water molecules	no. of Br ions	no. of $Si(OH)_3O^-$ molecules	no. of TMA^+ ions	final box size (nm)	concentration, mol/L
section 3.1	R1-DADDn	11	75	3753				5.17	0.9
	R2-DADDn	32	140	3130				5.20	1.65
	R3-DADDn	22	193	2320				5.12	2.39
	R4-DADDn	22	277	1452				5.17	3.33
	P1-DADDn	20	278	1452				5.13	3.42
section 3.2	P2-DADDn	22	140	3256				5.24	1.62
	R5-DADDs	20	142	3096	142			5.28	1.60
	P3-DADDs	20	142	3128	142			5.28	1.60
	R6-DADDd	20	140	3130	280			5.39	1.49
	P4-DADDd	15	130	2798	260			5.22	1.52
	P5-DADDd	20	100	3102	200			5.17	1.20
section 3.3	P6-DADDn-Si	26	140	1663		140	140	5.02	1.84
	P7-DADDs-Si	30	142	2467		142		5.13	1.75
	P8-DADDd-Si	20	130	1938		260		5.05	1.68

layers. The idea was to establish whether the layer represents the real equilibrium structure for the system under evaluation. In molecular dynamics, the equilibrium state is normally approached starting from random configurations; however, some systems might be affected by very slow dynamics, and reaching this equilibrium might be computationally very expensive. To overcome this problem, one can think of also approaching equilibrium from the opposite side, e.g. starting the simulation from a highly ordered state and following its evolution. If the preformed states do not correspond to equilibrium structures, then they should start collapsing quite rapidly and eventually become homogeneously dispersed in the system. However, if they are stable aggregates, then they will undergo only small internal rearrangements.

Details about the entire set of simulations performed, including length, number of molecules, and final box size, can be found in Tables 1 and 2. The first letter of the simulation name refers to how the system was created: R indicates that all of the molecules were randomly placed in the box at the start of the run, and P designates a simulation in which preformed layers of surfactants were used as the initial configuration. This letter is followed by a running number for each type of system analyzed. Then the type of surfactant used is provided, with DADDn used for neutral diaminododecane molecules, DADDs used for singly charged, and DADDd used for doubly charged. Finally, Si is added for simulations containing silica monomers. Input files of all of the simulations performed in this article are openly available though the Strathclyde data repository (DOI: 10.15129/f596b3b0-5285-46d2-8939-8a50aed20701).

Table 2. Simulation Details for Experimental Case

		R7-EXP-reference	P9-EXP-reference		P10-EXP-monomeric
name	%	no. of molecules	no. of molecules	%	no. of molecules
DADDn	~27	38	38	~25	35
DADDs	~45	63	63	~51	71
DADDd	~27	39	39	~24	34
Br ions		141	141		
TMA ions					112
water		2785	2784		1484
$Si(OH)_4$				~10	29
$Si(OH)_3O^-$				~90	251
time (ns)		100	20		91

The reference system was investigated first by considering the effect of an increase in concentration of neutral polyamine molecules in water (section 3.1). It should be noted that the ratio of surfactants to water species used to represent each concentration has been determined so that when the system reaches its equilibrium state the final box size is kept constant at approximately 5.2 nm in each direction. (See Table 1 for the details of each simulation run.) Next, the effect of a change in pH on this same system was investigated (section 3.2), and in order to establish a direct comparison with the previous set of simulations, only the concentration that produced a complete layer of neutral surfactants was used (simulation R2-DADDn). Once again, the number of water molecules was adjusted so that the final box size was kept approximately constant at equilibrium while the overall neutrality of the system was achieved by adding bromide counterions. The relative proportion of different surfactant species in the system was determined by considering specific pH conditions. Wang et al.[22] found that nonionic DADD molecules are present at high pH (above 11), singly charged DADD is present at pH between 8 and 11, and doubly charged species are found at pH lower than 8. Ohtaki and Maeda[23] determined the dissociation constants of several protonated diamines, among which is 1,12-diaminododecane, using potentiometric methods. These dissociation constants were used to obtain the titration curve for this system (Figure S1 in Supporting Information) through the utility CurTiPot.[24] In agreement with the results of Wang et al.,[22] the titration curve indicates that the fully charged and neutral species are dominant at the two extremes of the pH range, circum-neutral and high pH, respectively, whereas in the range of intermediate pH all three species are present in the approximate ratio of 50% for DADDs and 25% for both DADDn and DADDd.

The preformed layer structures used as starting configurations in the stability tests were created with the procedure described here. First, a layer containing surfactant molecules was made using Packmol software;[25] this allows us to build initial configurations such as lamellar, vesicles, and other ordered systems simply by placing molecules in the simulation box according to specific geometrical constraints. The size of the simulation box was chosen considering the equilibrium box size for the system obtained from corresponding random simulations. Then, the system containing only the preformed layer was relaxed, and other species, such as counterions and silica, were added and the system was solvated using a pre-equilibrated box of water as a source.

DOI: 10.1021/acs.langmuir.6b01731
Langmuir 2016, 32, 7228−7240

In the last part of our work, we analyzed the influence of the addition of anionic silica to preformed surfactant aggregates at different pH. The initial configurations were created with the procedure described above for the stability tests with the only difference that $Si(OH)_3O^-$ monomers were added instead of bromide counterions. It should be noted that when neutral surfactants are used, positive counterions need to be added to the system in order to balance the negative charge of the anionic silica species. Tetramethylammonium (TMA) ions are used for this purpose because we do not expect them to play an important role in the aggregation process.[15] The titration curve in Figure S2 was obtained in the same way as before but by including the pK_a for silicic acid,[26] and it shows that silica monomers are mostly in their neutral form at pH below 8 while at high pH they become anionic.

All of the simulations were performed using the GROMACS 4.6 package.[27] For all of the concentrations and pH values studied, production runs were performed in the NpT ensemble by keeping the temperature constant at 298.15 K with the Nosé−Hoover thermostat[28] and the pressure fixed at 1 bar by employing the Parrinello−Rahman barostat.[29] The equations of motion were integrated using the leapfrog algorithm[30] with a time step of 2 fs. The actual production simulations were preceded by an energy minimization step as well as two short equilibration simulations, first in the NVT and then in the NpT ensemble, the length of which depends on the time needed to equilibrate the system density. The simulation boxes were always cubic with periodic boundary conditions applied in the x, y, and z directions.

Water molecules were modeled using the SPC/E (extended simple point charge) potential,[31] a rigid three-site model widely used in MD simulations. Point charges are located on both the oxygen (Ow) and the two hydrogens (Hw), whereas only the oxygen atom has Lennard-Jones parameters. DADD surfactants are called bolaamphiphiles or two-headed amphiphiles. This term is used to describe molecules consisting of two headgroups separated by a long hydrocarbon chain.[32] To be more precise, a single DADD molecule contains, depending on the protonation state, 42 (DADDn, neutral surfactant), 43 (DADDs, singly charged surfactant), or 44 (DADDd, doubly charged surfactant) sites. A representation of the three surfactants used is provided in Figure 1: the amino group differentiates neutral surfactants from singly and doubly charged species.

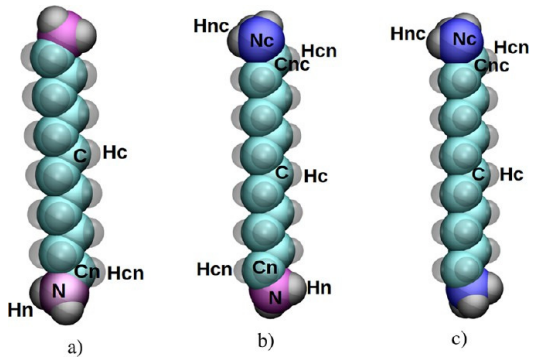

Figure 1. All-atom representations of the DADD surfactant in different charge states: (a) DADDn, (b) DADDs, and (c) DADDd. Neutral nitrogens, purple; charged nitrogens, blue; carbons, cyan; and hydrogens, gray.

Label Hn represents hydrogen atoms belonging to amino groups, with N indicating a nitrogen and Cn indicating a carbon bonded to it. The hydrogens on Cn atoms are referred as Hcn, and those on carbons C in the hydrocarbon chain are called Hc. When the surfactant heads are charged, the hydrogen atoms in the amino groups take the name Hnc; the nitrogens are indicated by Nc and the carbons bonded to them are indicated by Cnc. The OPLS (optimized potentials for liquid simulations) all-atom (AA) force field[33,34] is used to describe surfactants and counterions, such as bromide and TMA. This was validated against experimental properties, such as the liquid density and enthalpy of vaporization, by Caleman et al.[35] for several compounds, among which are simple amines. Parameters used for the neutral and anion silicic acid are taken from the work of Jorge et al.[17] Four different types of atoms are used to describe a molecule of $Si(OH)_3O^-$: the silicon atom (SiI), the oxygen atom belonging to the hydroxyl group (OhI), the hydrogen atom belonging to the hydroxyl group (HoI), and the charged oxygen atom (Oc). The potential energy function is represented as the sum of angle bending, dihedral torsion, Lennard-Jones interactions, and the Coulomb electrostatic term. Nonbonded interactions are calculated only for atoms that are separated by three or more bonds, and the 1−4 interactions are scaled down by a factor of 0.5. Bond lengths were constrained by applying the LINCS algorithm;[36] a cutoff of 1.2 nm was applied to short-range dispersion interactions and the same distance for the particle-mesh Ewald method (PME)[37,38] to take into account the long-range Coulomb electrostatics. Finally, a long-range dispersion correction term was added to both energy and pressure. Details of the entire set of parameters used can be found in Tables S1−S4 of the Supporting Information.

One of our objectives is to analyze the development of the surfactant aggregation process, with and without silica, in order to gain better insight into the role played by the latter. This means monitoring the evolution of the system over time and calculating characteristic properties such as the number of clusters and the average cluster size as well as the distribution of surfactant aggregates. For this purpose, an adaptation of the Hoshen−Kopelman cluster-counting algorithm[39] was used to analyze sampled trajectories. Two DADD molecules were considered to belong to the same cluster if the distance between at least one of the three central atoms (one carbon C and two hydrogens Hc) was less than 0.65 nm. We tested different criteria (for example, six central atoms instead of three) and values for the limiting distance between carbon/hydrogen atoms by visually inspecting distinct time frames of the system. The final value chosen provides the correct cluster size distribution for all types of surfactant molecules and is close to the position of the first minimum in the radial distribution function (RDF) between aliphatic hydrogen and carbon atoms (not shown here). The equation used to compute the number-average cluster size for clusters larger than four molecules is

$$\langle CN_N \rangle_4 = \frac{\sum_{n=4}^{\infty} n[M_n]}{\sum_{n=4}^{\infty} [M_n]} \quad (1)$$

where n indicates the size of the clusters and M_n is the concentration of clusters with n molecules.

For the simulations that produced layers, we calculated the interfacial tension to obtain an indication of the system tendency to evolve from layerlike structures into aggregates with higher interfacial areas, e.g., vesicles. This was done via the virial route[40,41] by calculating the pressure tensor using the utility *g_energy* in GROMACS[27] and averaging the values over the last 15 ns of the production run. It should be noted that each value must be divided by the number of surfaces, 2 in this case. Finally, all of the images presented were produced using VMD software.[42]

3. RESULTS AND DISCUSSION

3.1. Reference Solution: Effect of Concentration.

Understanding the process of formation of bioinspired mesoporous silica materials is the main objective of this work. However, to clearly assess the role played by both surfactants and silica species in the synthesis, we first need to examine in detail the self-assembly process of the polyamine molecules in the absence of silicates and under different concentration and pH conditions because it has not yet been addressed in the literature.

Figure 2 shows the equilibrium configurations obtained in the reference solution for an increasing concentration of neutral surfactant molecules (Table 1). We observe that highly ordered lamellar aggregates are formed only for the two intermediate

DOI: 10.1021/acs.langmuir.6b01731
Langmuir 2016, 32, 7228−7240

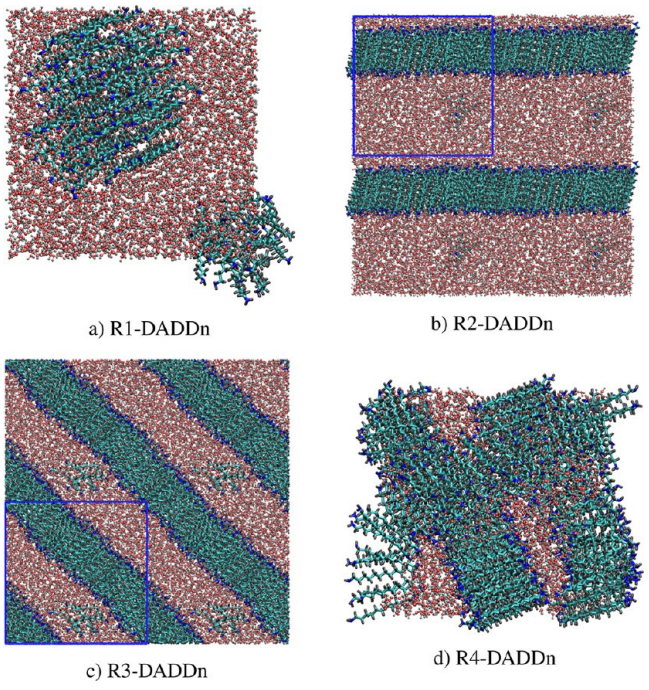

Figure 2. Snapshots of the 2D cross section of the simulation box at different concentrations: (a) R1-DADDn, (b) R2-DADDn, (c) R3-DADDn, and (d) R4-DADDn. Nitrogens, blue; hydrogens, gray; carbons, cyan; and oxygen, red. For clarity, periodic replicas have been added in (b) and (c) where the blue lines represent the boundaries of a single simulation box.

values of concentration, 1.65 and 2.39 mol/L (at the lower concentration, the aggregate formed appears to be a frustrated layer resulting from the finite size of the simulation box). Both layers appear to be completely dry and are composed, respectively, of 136 and 189 amine molecules. It is interesting to observe that when the number of surfactants is increased from 140 (R2-DADDn) to 193 (R3-DADDn) they tend to pack by maximizing the number of molecules that can be accommodated in a single layer. In a cubic box, this corresponds to a transition from a horizontal layer to a diagonal layer; in both cases, however, we observe a small number of dispersed monomers in equilibrium. When the number of surfactants is further increased to 277 (R4-DADDn), we would expect that the reciprocal interactions between aggregates would become more important and the system would evolve toward more ordered configurations.[43] However, what we observe is the formation of a less organized bicontinuous phase made of three incomplete tilted layers intersecting each other. One possibility is that the size and the shape of the simulation box might not allow us to observe the creation of a bilayer phase. This possibility can, however, be excluded because simulations of preformed bilayer systems (P1-DADDn) show that these aggregates remain stable in water (details in Figures S3 and S4 of the Supporting Information). A more likely possibility is that the bicontinuous phase observed in R4-DADDn could just represent an intermediate structure and the process leading to the creation of an ordered arrangement occurs too slowly for our atomistic simulations.

In Figure S5, we compare the evolution of the number-average cluster size over time for the systems represented in Figure 2. It should be noted that both equilibration steps (NVT and NpT) that preceded each MD production run are included in the cluster counting analysis; therefore, the total length of the simulation is slightly different from what is reported in Table 1. For what concerns the lower concentration (R1-DADDn), we note that the aggregation process occurs through three successive steps, each representing the fusion of two smaller clusters. In agreement with what we just discussed, we observe that the initial aggregation process is substantially faster when the number of surfactants is doubled (from R1-DADDn to R2-DADDn), and the system starts approaching the equilibrium value very quickly. This represents, in the case of R2-DADDn and R3-DADDn, the number of molecules that can be accommodated in a stable layer. Although increasing the concentration speeds up the initial aggregation process, the system requires more time to reach a fully ordered state, as in the case of the bicontinuous system (R4-DADDn).

3.2. Reference Solution: Effect of pH. Once the influence of the concentration on the aggregation process of DADD surfactants was understood, the effect of pH (i.e., the charged state of the surfactant molecules) on the structure and types of aggregates formed was studied. This is a very important aspect because the hydrophobic/hydrophilic character of the surfactant molecules and therefore their interactions with silicate species will depend on their charged state. We focus on the surfactant concentration that potentially leads to the formation of single horizontal layers (approximately 1.6 mol/L, cf. Table 1).

Figure 3 shows the final configurations obtained, in the case of neutral surfactants, starting from a preformed layer (a) and

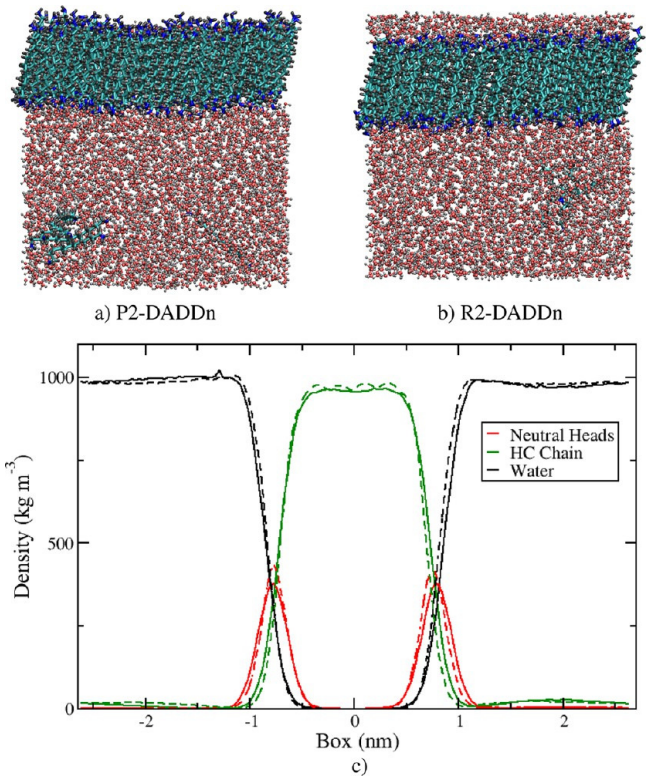

Figure 3. Snapshots of the 2D cross section of the simulation box for (a) P2-DADDn and (b) R2-DADDn and corresponding equilibrium density profiles across the box (c), starting from random initial configurations of surfactants (R2-DADDn, solid line) and from a preformed layer (P2- DADDn, dashed line). The color code is the same as in Figure 2.

DOI: 10.1021/acs.langmuir.6b01731
Langmuir 2016, 32, 7228−7240

from an initially random system (b). The two layers are practically identical as shown by looking at the density profiles across the box (Figure 3c). The central part of the layer is occupied by the hydrocarbon chains, which in turn create, as a result of their strong hydrophobic character, a water depletion region. The neutral heads are localized at the interface with water where they establish favorable hydrophilic interactions. In Figure S6, a comparison between the number of clusters and the number-average cluster size calculated for the two systems demonstrates that they both evolve toward the same final equilibrium values. It is worth noting that the number-average cluster size computed for the preformed system is essentially constant, implying that the layer does not undergo any major rearrangement. This confirms that DADD neutral surfactants form stable layer structures in water.

In Figure 4, we show the results of simulations with singly charged surfactants, comparing the final configurations

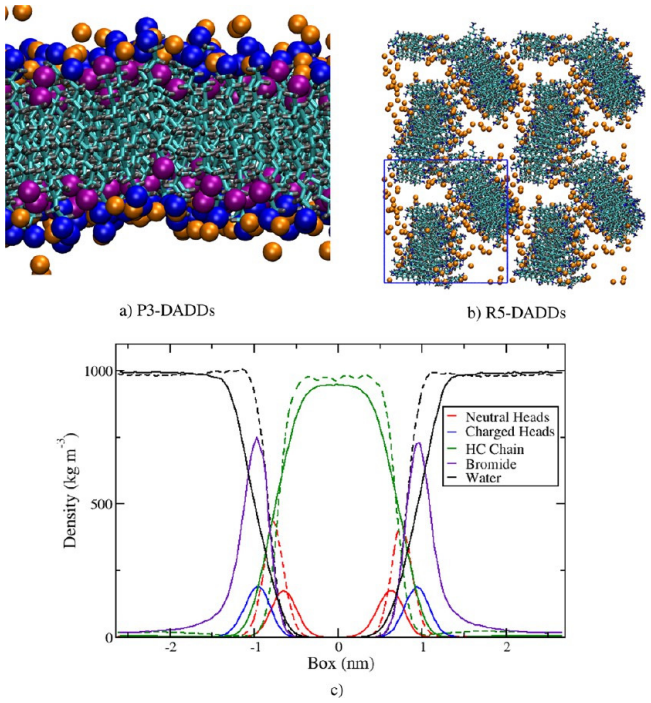

Figure 4. (a) Snapshot of the 2D cross section of the simulation box obtained for P3-DADDs showing the detail of the layer. (b) Snapshot of the 2D cross section of the simulation box obtained for R5-DADDs starting from a random initial configuration of surfactants. (c) Comparison between the density profiles across the box in the singly charged system (P3-DADDs, solid line) and in the neutral system (P2-DADDn, dashed line). The color code is the same as in Figure 3 with bromide being orange, charged nitrogens being blue, and neutral nitrogens being purple. Periodic replicas have been added in (c), where the blue lines represent the boundaries of a single simulation box. Water molecules are not shown for clarity.

obtained starting from preformed layers (a) and from random configurations (b). Although the random system did not produce a complete layer, we observed the formation of large ordered structures after approximately 5 ns (Figure 4b). These separate blocks are likely to merge to form a layer similar to the one we observed in the neutral system. Time limitations might not allow us to obtain the equilibrium structures, but our simulations with preformed layers can help identify possible stable states for this system. We found that a layer of DADDs surfactant contains 141 molecules (5 more than a layer of neutral surfactants) in approximately the same size box (Figure 4a). More information about the singly charged system can also be extracted by looking at the evolution of the number of clusters and the number-average cluster size in Figure S7. The trajectory of the random simulation (R5-DADDs) was analyzed and compared to the one produced using the preformed layer for the same concentration of surfactants (P3-DADDs). The first trajectory seems to approach but does not really reach the final equilibrium value of 141 molecules packed in the layer. The aggregation process takes place by successive fusion steps similar to what we observed in the neutral system for the lowest concentration. The larger these aggregates are, the more stable they become and therefore the longer it takes for them to merge into larger structures. This behavior is also reflected in the evolution of the total number of clusters: it rapidly decreases at the very beginning of the simulation and then, after approximately 5 ns, essentially oscillates at very low numbers (mainly between four and two) because of molecules that temporarily leave the two major aggregates. It is thus reasonable to expect to see a complete layer form after a long simulation time, and this is supported by the fact that the preformed layer is very stable in water during a long MD trajectory.

A detail of the final configuration obtained for P3-DADDs is provided in Figure 4a. Here a different color code has been used to distinguish between charged and neutral heads (blue and purple, respectively). The two types of heads appear to be alternating in the lamellar structure, with the charged groups in close contact with the bromide ions while the neutral heads are located slightly below the interface with water. This arrangement produces the minimum repulsion interactions between the charged headgroups and, at the same time, makes the layer more compact so that more surfactant molecules can fit inside it. Another interesting feature is that the DADDs molecules inside the layer seem to have a straighter conformation in comparison to the neutral DADD molecules, which appear to be slightly tilted in Figure 3. This change in conformation could be related to the surface tension and will be discussed later.

Figure 4c compares neutral and singly charged layer density profiles. In both layers, the hydrocarbon chains are located in the central part of the layer, producing a dry region. The shape of the singly charged profile is, however, slightly different compared to its counterpart in the neutral system: the peak appears to be narrower and the tails of the distribution extend further than in the neutral system. This is due to the alternating arrangement of surfactant heads in the layer, causing the neutral heads to slide toward the middle part of the layer while the charged ones prefer to stay at the interface. It is also worth noting that the peak corresponding to the head density distribution for the DADDn system is located at the midpoint between neutral and charged head profiles belonging to the DADDs system. The interface itself is in general more structured in the latter system because of the presence of bromide counterions. Bromide peaks essentially overlap with the charged head peaks, causing the water layer to move back (in comparison to the neutral system) while increasing the depletion region around the hydrocarbon chain.

In Figure S9, we analyze RDFs between different regions to gain more insight into the structures resulting from DADDs surfactant aggregation. Both charged and neutral heads (solid lines) exhibit stronger interactions with water in the incomplete layer, and as we would expect, the magnitude of these

DOI: 10.1021/acs.langmuir.6b01731
Langmuir 2016, 32, 7228−7240

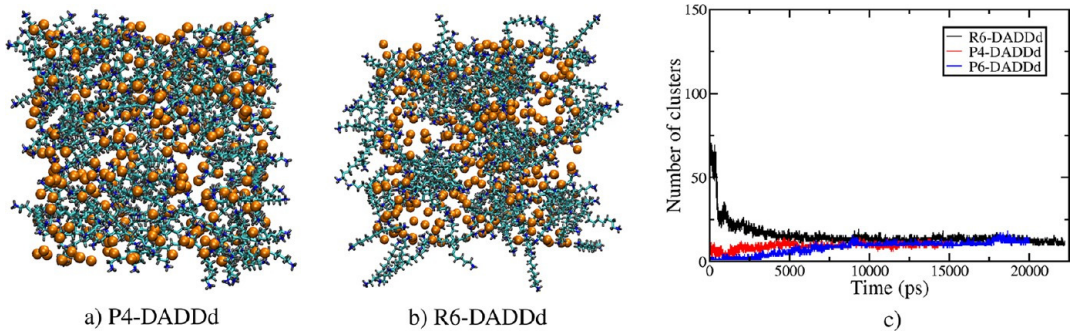

Figure 5. Snapshot of the 2D cross section of the simulation box of P4-DADDd (a) and comparison with the 2D cross section of the simulation box of R6-DADDd (b). The layer made with Packmol is quickly destroyed. (c) Comparison between the number of clusters obtained for the reference solutions with DADDd surfactants at different concentrations: R6-DADDd, black; P4-DADDd, red; and P5- DADDd, blue. The color code is the same as in Figure 4. Water has been removed for clarity.

interactions is higher for positively charged nitrogens (Figure S9a,b). On the other hand, the increase in order and compactness in the complete layer favors the interactions between nitrogens and bromide ions as well as among headgroups (Figure S9c,d). All of the RDFs calculated between headgroups show a main peak located at approximately 0.5 nm with a very similar magnitude of interaction, confirming the regular alternating arrangement of surfactant molecules in the layer we described by visual inspection of the final snapshots.

Figure 5 shows the equilibrium configuration obtained with a preformed layer of doubly charged surfactant molecules (P4-DADDd, a) and with random initial configurations (R6-DADDd,b). The final results appear to be very similar: the preformed layer starts breaking apart very quickly, and it is practically entirely destroyed after the first 5 ns of simulation time, as shown in Figure S8, while the random system produced only small aggregates. This is due to the stronger repulsion between surfactant headgroups in this system, which tends to favor interactions with water. The high solubility of DADDd molecules results in a much lower value of the number-average cluster size and no evidence of the formation of lamellar structures. Interestingly, the same behavior was also found for a layer built with a lower concentration of surfactants (see the results for simulation P5-DADDd) where a weaker repulsion between heads is expected.

We observe these small aggregates to be quite disordered, only loosely resembling spherical micelles commonly formed with single-head surfactants.[15] It is also interesting that all the simulations performed, with three different concentrations of doubly charged surfactants and starting from either random or preformed layers, converge to a similar value for the number-average cluster size as displayed in Table 3. The RDFs in Figure S10 help explain why, in contrast to the neutral and singly charged systems, it was not possible to produce a stable layer of DADDd molecules. The interactions between charged heads and bromide ions are weaker in the doubly charged system than in the DADDs system (Figure S10c). At the same time, we note that the interaction of the charged group with water is comparable in the two systems. These observations suggest that the lack of order in the system lowers the peak of the head-bromide RDFs.

Table 3. Number-Average Cluster Size for R6-DADDd, P4-DADDd, and P5-DADDd

name	average cluster size
R6-DADDd	12.74
P4-DADDd	17.61
P5-DADDd	11.04

The head-to-head repulsion plays a crucial role in determining equilibrium in these systems.[32] The aggregation of two-headed amphiphiles depends, in fact, on three contributions: the attraction between the hydrocarbon chains, the hydrophobic interactions of these chains with water at the interface, and the repulsions between polar heads. The first two terms both favor the formation of large aggregates as a result of the dispersive attractions between hydrophobic groups and the tendency to minimize the interface with water. On the other hand, the last contribution limits the size of these aggregates due to the repulsion between polar heads, which becomes greater with their increasing proximity. For neutral heads, this term is small compared to the other two. In DADDs, it is minimized through the alternating arrangement observed in Figure 4a. In DADDd, however, it dominates the other two terms, leading to layer breakup and the formation of small disordered clusters (Figure 5c). Figure S10d confirms that for this system the interaction between charged heads is indeed strongly repulsive.

Further support for these observations is given by the energies of interaction calculated for the three preformed systems {P2-DADDn (neutral), P3-DADDs (singly charged), and P4-DADDd (doubly charged)}, as summarized in Table S5. Coulombic and Lennard-Jones contributions to the total energy are compared in the three systems for three types of interactions: surfactant−surfactant, surfactant−water, and surfactant−bromide. It is worth noting that the values obtained using the utility *g_energy* have been normalized by the number of surfactant molecules or bromide ions in each system in order to perform a comparison on a equal basis. The first thing to notice is that the total surfactant−surfactant interaction energy is, as expected, attractive in the case of neutral and singly charged surfactants but repulsive in the case of doubly charged surfactants. In all three systems, the Coulombic contribution to the total energy is repulsive and its magnitude increases with increasing charge of the surfactants; however, dispersion interactions more than compensate for this in P2-DADDn and P3-DADDs but not in P4-DADDd (details in Table S5). These results are consistent with the first two systems forming lamellar aggregates, whereas the third one forms only small clusters.

So far, each of our simulations has considered only a single type of surfactant for simplicity. In reality, as will be further

DOI: 10.1021/acs.langmuir.6b01731
Langmuir 2016, 32, 7228−7240

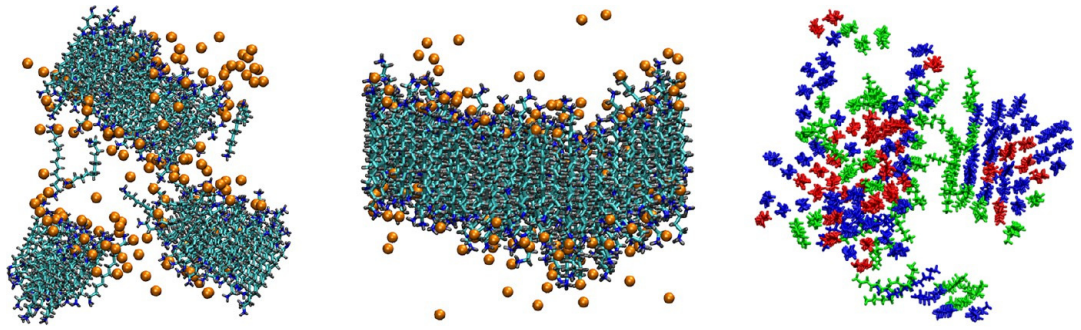

Figure 6. Snapshots of a 2D cross section of the simulations corresponding to experimental conditions in the reference solution (a) starting from a random configurations of surfactants and (b) starting from a preformed layer with randomly arranged surfactants. The color code is the same as in Figure 4. (c) Top view of the layerlike aggregate in (a) to show that all types of surfactants are incorporated into the layer (DADDn, red; DADDs, blue; and DADDd, green).

discussed in section 3.4, all three types of surfactants coexist at intermediate pH values (between 9 and 12), with DADDs being the most abundant species (approximately 50%) as shown from the pH curves in Supporting Information (Figures S1 and S2). Although Tanev and Pinnavaia do not report the pH of their synthesis solution,[11] we have estimated this to be 9.5 on the basis of the starting composition of the mixture. As such, to more closely model the experimental scenario, we have decided to run simulations at a pH of 10.6, which is slightly higher than the experimental value but more convenient from a modeling point of view because DADDn and DADDd surfactants are present in equal proportions so that they can balance each other. The reference system was studied starting from a random dispersion of surfactants (R7-EXP-reference) or from a preformed layer (P9-EXP-reference). The latter was built by packing DADDn, DADDs, and DADDd molecules, according to the proportion reported in Table 2, in a layer geometry without any preferred distribution, so their lateral arrangements were as arbitrary as possible.

Figure 6 shows the final configurations obtained in these simulations. The first thing we notice is that, because of slow dynamics, the random system (Figure 6a) did not produce a complete layer after 100 ns. However, as can be seen in Figure 6c, all three types of surfactants are incorporated in growing layerlike aggregates. These seem to be positioned without any specific preference inside the structures formed because we do not observe any domains where one type of surfactant remains separate from the others.

Furthermore, it appears that these aggregates might merge together to form a single layer for longer simulation times. This hypothesis was tested using the preformed layer simulation, and the result is shown in Figure 6b. The preformed layer keeps its integrity, validating the hypothesis that the distinct aggregates observed previously will eventually merge together. We also notice that the interface is no longer perfectly flat but exhibits a quite pronounced undulation. The reasons for this wavy interface will be discussed in the next section.

3.3. Monomeric Solution. In this section, we discuss the results obtained from the addition of anionic silica to preformed surfactant layers at different pH values (Table 1).

The first thing we notice by looking at Figure 7 is that the addition of silica anions appears to keep the layers intact when neutral (a) or singly charged (c) surfactants are used, whereas for the system with doubly charged surfactants (e) the presence of silica species does not enhance any structural organization.

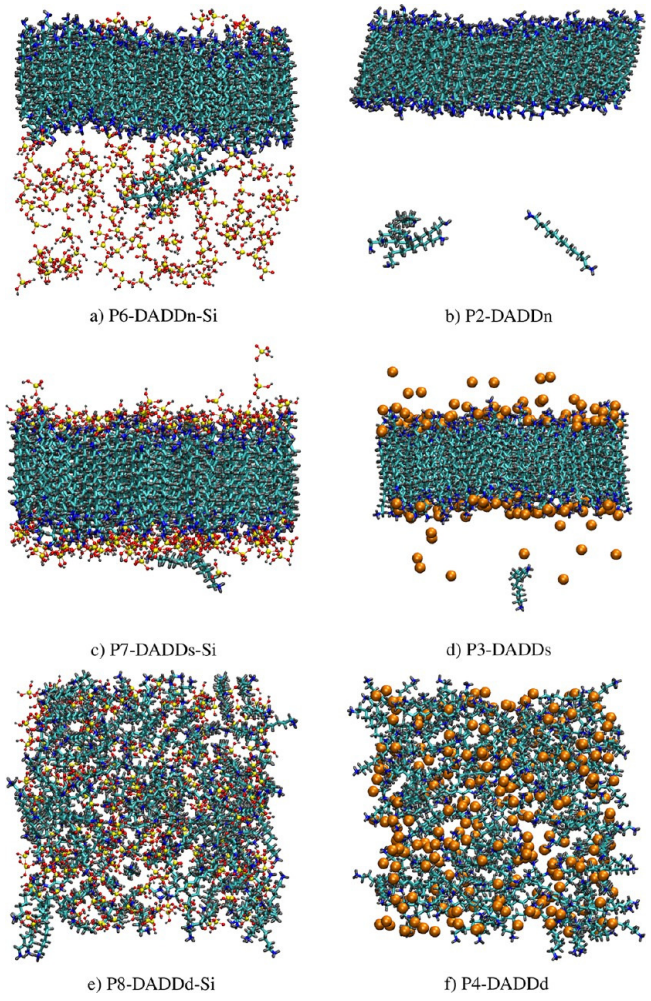

Figure 7. Snapshots of the 2D cross section of the simulations for different monomeric solutions (left) in comparison with configurations obtained in the case of the reference system (right): (a) P6-DADDn-Si, (b) P2-DADDn, (c) P7-DADDs-Si, (d) P3-DADDs, (e) P8-DADDd-Si, and (f) P4-DADDd. The color code is the same as in Figure 4a, with silicon being yellow. Water is omitted for clarity.

With regard to this last system, typical clusters produced in the reference system and in the monomeric solution are compared in Figure 8. An analysis of these aggregates, both by visual inspection and using the cluster-counting algorithm, reveals

DOI: 10.1021/acs.langmuir.6b01731
Langmuir 2016, 32, 7228−7240

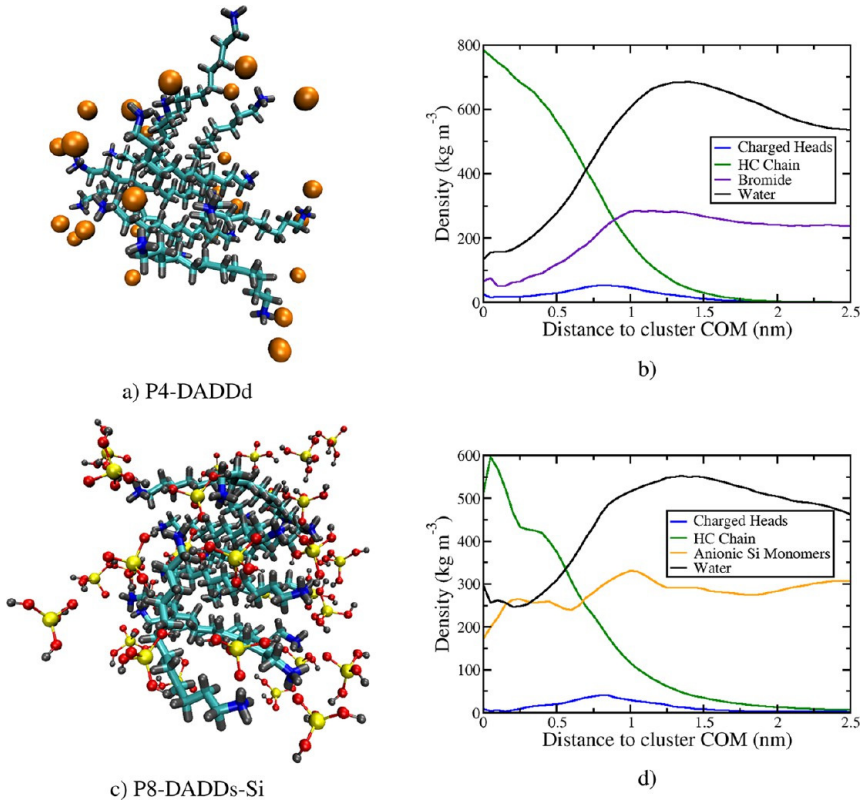

Figure 8. Snapshots of two clusters, both containing nine surfactant molecules each, obtained for P4-DADDd (a) and P8-DADDd-Si (c), as well as corresponding density profiles, (b) and (d), respectively. The color code is the same as in Figure 7. Water is omitted for clarity.

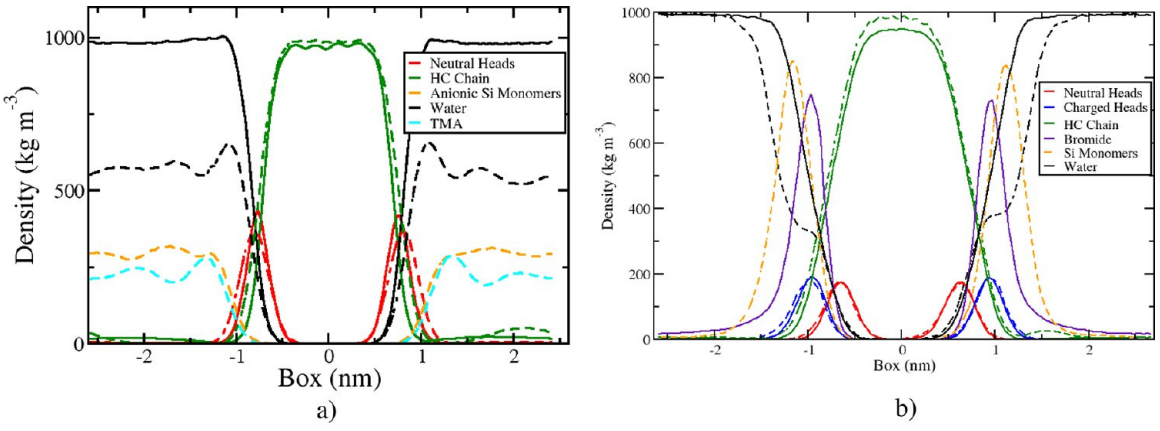

Figure 9. (a) Comparison of density profiles across the box for the neutral system, reference solution P2-DADDn (solid line), and monomeric solution P6-DADDn-Si (dashed line). (b) Comparison of density profiles across the box for the singly charged system in the reference solution P3-DADDs (solid lines) and in the monomeric solution P7-DADDs-Si (dashed lines).

that they are very similar in size (from 7 up to 13 DADDd molecules in each cluster) and are surrounded by a comparable number of ions. When we look at the density profiles (Figure 8b,d) measured from the cluster center of mass (COM), we notice that they present very little order and only vaguely resemble micelle density profiles. In fact, the core of the clusters contain the hydrophobic chains of the molecules but also a few water molecules and ions, both in the reference system and in the monomeric solution. Moreover, we notice that the peak representing the heads of the surfactants is located at the interface with water but is quite broad as a result of the disordered nature of these aggregates.

Concerning the system containing neutral surfactants, when silica species are added the layer remains intact and the monomers are homogeneously dispersed in the bulk solution (Figure 7a). In Figure 9a, we compare the density profiles of this system in the reference solution (solid line) and in the monomeric solution (dashed line). The lamellar layers of surfactants are practically identical in both systems, proving that no major structural changes have occurred. Looking at the area immediately around the layer, past the neutral heads, we notice, in the case of the monomeric solution, a region of approximately 0.5 nm in size where mostly water molecules are present, indicating the presence of a wet layer around the surfactants. Finally, TMA and silica monomers are found

DOI: 10.1021/acs.langmuir.6b01731
Langmuir 2016, 32, 7228−7240

homogeneously dispersed in the bulk of the solution, reducing the overall density of water in comparison to that in the neutral system. These results suggest a stronger interaction between silica monomers and water rather than with the surfactants.

This behavior is confirmed by looking at the RDFs for the system in Figure S11. Clearly, the peak representing the interactions between the TMA nitrogens and the silicon atoms is the predominant one, located at approximately 0.55 nm, whereas the peak relative to the interactions between surfactant nitrogens and silica is very low in comparison (Figure S11a). This is caused by the comparatively strong electrostatic interaction between positively charged TMA molecules and anionic silica monomers. The second thing we notice is the location of the different peaks representing the interaction between surfactant nitrogens and oxygen atoms in water (Ow) and in silica (OhI is the oxygen belonging to the hydroxyl group and Oc is the charged oxygen), as shown in Figure S11b. The N-Ow peak is quite strong and occurs at a short distance, characteristic of hydrogen bond interactions. Conversely, there is practically no interaction between N and the charged oxygen of silica. The N-OhI peak is also very small (below 1) and probably caused by the few DADDn molecules dispersed in the bulk solution. These results provide additional evidence for the presence of the wet layer and suggest that hydrogen bonding interactions between the surfactant amino group and silica monomers are at best quite weak and therefore not sufficient to promote silicates to adsorb and then condense around these lamellar templates (Figure 7a).

Finally, in the system containing singly charged surfactants, contrary to the previously discussed case, silica monomers strongly interact with the surfactant headgroups, resulting in their adsorption at the interface (Figure 7c). If we look at the density profiles across the box (Figure 9b), we also notice that the presence of silica dries the interface in comparison to the reference system. This seems to be in qualitative agreement with the mechanism postulated experimentally for the formation of this class of materials.[11] However, given the charged nature of all of the species in our system, charge matching, rather than hydrogen bond interactions, appears to be responsible for the creation of the silica layer at the interface with DADDs surfactants.

To elucidate this point further, it is worth looking at the energies of interactions calculated for P6-DADDn, P7-DADDs, and P8-DADDd in Table S6. Here, Coulombic and Lennard-Jones contributions are shown for surfactant−surfactant, surfactant−water, and surfactant−silica interactions, with the appropriate normalization (number of surfactant or silica molecules) to allow direct comparison on a equal basis. The surfactant−surfactant interaction energies have the same trend as in the reference system: dispersion interactions more than compensate for the repulsive Coulombic interactions only in the systems that produced stable layers (i.e., P6-DADDn and P7-DADDs). The surfactant−silica interactions also show an interesting trend. In the neutral system, this energy is only moderately attractive because most of the silica monomers remain dispersed in the simulation box, favoring instead the interaction with water molecules. On the contrary, silica monomers strongly interact with surfactants in both singly and doubly charged systems (the surfactant−silica energy is −312.79 and −322.33 kJ/mol, respectively); however, in the first case, this interaction is with lamellar structures (surfactant−surfactant energy = −3.48 kJ/mol), and in the second case, it is with small clusters of surfactants (surfactant−surfactant energy = 90.87 kJ/mol). This further confirms the qualitative results discussed above.

3.4. Simulations at pH Close to Experiment. The simulations discussed in the previous section strongly suggest that the mechanism postulated for the formation of MSU-V materials can take place only when singly charged surfactants and anionic silicates are available in the system to establish favorable electrostatic interactions while keeping to a minimum the repulsion between charged heads.

In this section, we present results from simulations performed at an intermediate pH of 10.6, slightly higher than the estimated experimental pH, and considering a 2:1 ratio of silica monomers to surfactants (details in Table 2); i.e., each surfactant head can theoretically interact on average with one silicate. The reference system has already been presented in section 3.2 and will be used for comparison with the monomeric solution under the same set of conditions. As in the reference system, a preformed layer containing all the three types of surfactants but with no particular lateral arrangement was used as the initial configuration. All of the simulations were performed using the same parameters as described in section 2.

Because of the limited size of our atomistic simulations, only layers have been observed to form. However, multilamellar vesicles are expected to form in larger systems.[11] To analyze this possibility, we report an interesting feature that was observed during our analysis. We noticed that the orientation of the DADD molecules in the layers and the degree of undulation of the layer changed with the presence of silica (e.g., compare Figure 7a,b). These differences are believed to be related to the interfacial tension in the system. In Table 4, we report the values of the interfacial tension calculated for the simulations that produced a complete layer.

Table 4. Calculated Interface Tension

name	γ (mN m^{-1})	error (mN m^{-1})
R2-DADDn	36.89	3.45
P2-DADDn	40.53	0.19
P6-DADDn-Si	−35.66	1.85
P3-DADDs	31.56	1.5
P7-DADDs-Si	−23.40	3.4
P9-EXP-reference	−70.33	2.2
P10-EXP-monomeric	−82.77	4.65

The value of the interfacial tension assumes negative values in the systems containing silica species but also in the reference system when all three types of surfactants are present. This might appear to be an unphysical result; however, experimental[44] and computational[45,46] studies suggest that negative interfacial tension is an indication of an unstable surface. Therefore, the interfacial area will tend to increase, either by a change in the surface curvature or by mixing. The first possibility could be an indication that the system wants to evolve toward the formation of vesicles. The size and length of our simulations does not allow us to provide a conclusive answer to this question, and a more complete picture can be achieved using only coarse-grained molecular dynamics.

Looking at Figure 10a we notice that, similar to what was observed for the reference system, the preformed layer keeps its integrity while producing a very distinctive curvature. This observation seems to be in agreement with our surface tension calculations (Table 4), providing another indication that the

DOI: 10.1021/acs.langmuir.6b01731
Langmuir 2016, 32, 7228−7240

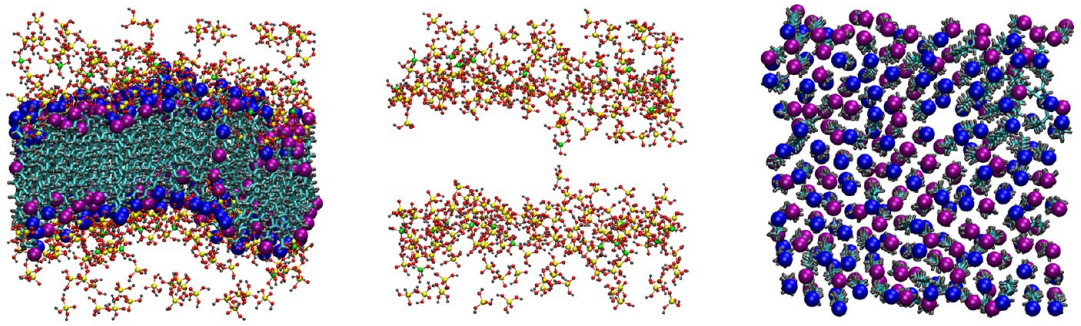

Figure 10. Snapshots of 2D cross section of the simulations corresponding to experimental conditions in the monomeric solution, starting from a preformed layer with randomly arranged surfactants: (a) side view of the layer with silica monomers adsorbed at the interface, (b) side view of the silica layers with silica monomers penetrating the hole in the surfactant layer, and (c) top view showing the location of the hole. Color code is the same as in Figure 4 with silicon in anionic silica being yellow and silicon in neutral silica being green.

system wants to evolve toward the creation of lamellar vesicles around which silicates precipitate.

Another thing to notice is that the layer presents a hole as can be clearly seen in Figure 10c, where a top view of the layer is shown. This structure is reminiscent of pore formation in biological membranes.[47] Interestingly, anionic and neutral silica monomers have been observed to spontaneously migrate into this hole (Figure 10b). A visual inspection of the simulation trajectory reveals that, in this region, four DADDd and two DADDs molecules are located in close proximity. This corresponds to six neighboring positively charged heads on one side of the layer and four on the opposite side. Hence, this local excess of positive charges triggers the creation of the hole, making the cavity accessible to small water molecules (up to two water molecules have been observed to temporarily occupy the hole) and to silica monomers, which penetrate the layer from both sides (i.e., from the upper part and from the lower part of the layer). The presence of local defects, such as the one observed in our simulation, could help explain how the interconnecting pillars reported experimentally are created. Tanev and Pinnavaia[10] suggest that silicates can penetrate the multilamellar surfactant vesicles, initiating silica growth also in the vertical direction, so that eventually two consecutive horizontal layers become connected. Therefore, one can imagine that similar holes or defects will form across the lamellar plane with more silicates migrating inside them. These cavities will become progressively full of silica monomers that will eventually condense and remain trapped inside the template structure. Ultimately, silica polymerization inside these cavities will generate the vertical pillars that connect the horizontal layers. We must consider, however, that several defects of this type are probably needed to maintain the structural integrity of the multilamellar framework. Confirming this hypothesis is way beyond the limitations of our atomistic simulations.

4. CONCLUSIONS

By performing detailed molecular dynamics simulations of 1,12-diaminododecane surfactants (DADD) in water (reference system) and in the presence of silicates (monomeric solution), we have investigated the concentration and pH dependence of the aggregation process that leads to the formation of MSU-V materials. Dry lamellar structures were obtained in the system containing only neutral DADD surfactants (pH > 11) starting from random configurations as well as when preformed layers are used as inputs, indicating that these aggregates represent stable equilibrium states. When surfactants are singly charged (at pH between 8 and 11), the same types of structures are produced, as established in our simulations starting from preformed layers. However, in this case surfactant molecules adopt an alternating arrangement inside the layer that can minimize the repulsion between charged heads. This strong electrostatic repulsion is, in fact, responsible for the breakage of the preformed layers at low pH when DADD surfactants are doubly charged, generating highly disordered aggregates consisting of small clusters rather than layers.

Notably, the addition of silica monomers to the doubly charged system does not enhance structural organization or change the average cluster size. Conversely, at high pH (>11) the layer is kept intact, but silicates remain homogeneously dispersed in the solution and no significant interaction occurs between silica and surfactant. At intermediate pH values (8–11), on the other hand, strong electrostatic interactions are established at the layer interface between anionic silicates and surfactant heads. This suggests that these simulations represent a state that more closely resembles the synthesis conditions leading to the formation of MSU-V materials. Contrary to what was originally hypothesized,[11] our simulations show that charge-matching interactions rather than hydrogen bonds promote silica adsorption around the amine template.

Our simulations at a pH close to the experimental value show that silicate adsorption at the interface induces a considerable curvature in the layer comprising all three types of surfactants (neutral and singly and doubly charged). We hypothesize that these systems are in a temporary frustrated state and want to evolve toward the formation of aggregates with higher interfacial areas, i.e., vesicles, in agreement with the multilamellar aggregates described experimentally.

Finally, we observed that a few silicates, together with water molecules, penetrated a hole spontaneously created inside the multisurfactant layer. This observation represents direct evidence of the intercalated pillaring mechanism proposed experimentally. Our hypothesis is that the presence of a local excess of charge triggers the formation of defects that become accessible to water and silica molecules; progressively, these holes or defects are filled with silicates that will eventually condense inside the templating structure, leading to the formation of vertical pillars connected to the horizontal silica layers at the interface with water. In future work, we intend to study this system on a larger scale by applying a coarse-graining

DOI: 10.1021/acs.langmuir.6b01731
Langmuir 2016, 32, 7228–7240

approach, currently under development, which should allow us to reach sufficient sizes and longer time scales to clarify some of the questions raised herein.

■ ASSOCIATED CONTENT

Supporting Information

The Supporting Information is available free of charge on the ACS Publications website at DOI: 10.1021/acs.langmuir.6b01731.

Force field parameters, titration curves, details of the bilayer test, cluster counting analysis, additional RDFs, and energy calculations (PDF)

■ AUTHOR INFORMATION

Corresponding Author

*E-mail: miguel.jorge@strath.ac.uk. Phone: +44 1415482825.

Notes

The authors declare no competing financial interest.

■ ACKNOWLEDGMENTS

We are grateful for funding from EPSRC UK Project Grant EP/L014297/1. A.C. acknowledges the University of Strathclyde for a Ph.D. studentship. Results were obtained using the ARCHIE-WeSt High Performance Computer (www.archie-west.ac.uk) funded by EPSRC grant no. EP/K000586/1.

■ REFERENCES

(1) Sun, Q.; Vrieling, E. G.; van Santen, R. A.; Sommerdijk, N. A. J. M. Bioinspired synthesis of mesoporous silicas. *Curr. Opin. Solid State Mater. Sci.* **2004**, *8*, 111−120.

(2) Tréguer, P.; Nelson, D. M.; Bennekom, A. J. V.; DeMaster, D. J.; Leynaert, A.; Quéguiner, B. The Silica Balance in the World Ocean: A Reestimate. *Science* **1995**, *268*, 375−379.

(3) Patwardhan, S. V. Biomimetic and bioinspired silica: recent developments and applications. *Chem. Commun.* **2011**, *47*, 7567−7582.

(4) Kröger, N.; Deutzmann, R.; Sumper, M. Polycationic Peptides from Diatom Biosilica That Direct Silica Nanosphere Formation. *Science* **1999**, *286*, 1129−1132.

(5) Sumper, M.; Brunner, E. Learning from Diatoms: Nature's Tools for the Production of Nanostructured Silica. *Adv. Funct. Mater.* **2006**, *16*, 17−26.

(6) Shimizu, K.; Cha, J.; Stucky, G. D.; Morse, D. E. Silicatein Îś: Cathepsin L-like protein in sponge biosilica. *Proc. Natl. Acad. Sci. U. S. A.* **1998**, *95*, 6234−6238.

(7) Sumper, M. A Phase Separation Model for the Nanopatterning of Diatom Biosilica. *Science* **2002**, *295*, 2430−2433.

(8) Beck, J. S.; Vartuli, J. C.; Roth, W. J.; Leonowicz, M. E.; Kresge, C. T.; Schmitt, K. D.; Chu, C. T. W.; Olson, D. H.; Sheppard, E. W. A new family of mesoporous molecular sieves prepared with liquid crystal templates. *J. Am. Chem. Soc.* **1992**, *114*, 10834−10843.

(9) Vrieling, E. G.; Sun, Q.; Beelen, T. P. M.; Hazelaar, S.; Gieskes, W. W. C.; van Santen, R. A.; Sommerdijk, N. A. J. M. Controlled silica synthesis inspired by diatom silicon biomineralization. *J. Nanosci. Nanotechnol.* **2005**, *5*, 68−78.

(10) Tanev, P. T.; Pinnavaia, T. J. Biomimetic Templating of Porous Lamellar Silicas by Vesicular Surfactant Assemblies. *Science* **1996**, *271*, 1267−1269.

(11) Tanev, P. T.; Liang, Y.; Pinnavaia, T. J. Assembly of Mesoporous Lamellar Silicas with Hierarchical Particle Architectures. *J. Am. Chem. Soc.* **1997**, *119*, 8616−8624.

(12) Auerbach, S. M.; Fan, W.; Monson, P. A. Modelling the assembly of nanoporous silica materials. *Int. Rev. Phys. Chem.* **2015**, *34*, 35−70.

(13) Siperstein, F. R.; Gubbins, K. E. Phase Separation and Liquid Crystal Self-Assembly in Surfactant-Inorganic-Solvent Systems. *Langmuir* **2003**, *19*, 2049−2057.

(14) Jin, L.; Auerbach, S. M.; Monson, P. A. Simulating the Formation of Surfactant-Templated Mesoporous Silica Materials: A Model with Both Surfactant Self-Assembly and Silica Polymerization. *Langmuir* **2013**, *29*, 766−780.

(15) Jorge, M. Molecular Dynamics Simulation of Self-Assembly of n-Decyltrimethylammonium Bromide Micelles. *Langmuir* **2008**, *24*, 5714−5725.

(16) Jorge, M.; Gomes, J. R. B.; Cordeiro, M. N. D. S.; Seaton, N. A. Molecular Simulation of Silica/Surfactant Self-Assembly in the Synthesis of Periodic Mesoporous Silicas. *J. Am. Chem. Soc.* **2007**, *129*, 15414−15415.

(17) Jorge, M.; Gomes, J. R. B.; Cordeiro, M. N. D. S.; Seaton, N. A. Molecular Dynamics Simulation of the Early Stages of the Synthesis of Periodic Mesoporous Silica. *J. Phys. Chem. B* **2009**, *113*, 708−718.

(18) Marrink, S. J.; de Vries, A. H.; Mark, A. E. Coarse Grained Model for Semiquantitative Lipid Simulations. *J. Phys. Chem. B* **2004**, *108*, 750−760.

(19) Marrink, S. J.; Risselada, H. J.; Yefimov, S.; Tieleman, D. P.; de Vries, A. H. The MARTINI Force: Field: Coarse Grained Model for Biomolecular Simulations. *J. Phys. Chem. B* **2007**, *111*, 7812−7824.

(20) Pérez-Sánchez, G.; Gomes, J. R. B.; Jorge, M. Modeling Self-Assembly of Silica/Surfactant Mesostructures in the Templated Synthesis of Nanoporous Solids. *Langmuir* **2013**, *29*, 2387−2396.

(21) Pérez-Sánchez, G.; Chien, S.-C.; Gomes, J. R. B.; D.S. Cordeiro, M. N.; Auerbach, S. M.; Monson, P. A.; Jorge, M. Multiscale Model for the Templated Synthesis of Mesoporous Silica: The Essential Role of Silica Oligomers. *Chem. Mater.* **2016**, *28*, 2715.

(22) Wang, F.; SHI, Z.; GONG, F.; JIU, J.; ADACHI, M. Morphology Control of Anatase TiO2 by Surfactant-assisted Hydrothermal Method. *Chin. J. Chem. Eng.* **2007**, *15*, 754−759.

(23) Ohtaki, H.; Maeda, M. Ionic Equilibria in Mixed Solvents. VIII. Solvent Effects on the Dissociation of Diprotic Acids in Aqueous Methanol Mixtures. *Bull. Chem. Soc. Jpn.* **1973**, *46*, 2052−2056.

(24) Gutz, I. G. R. *CurTiPot*; pH and Acid Base Titration Curves: Analysis and Simulation freeware, version 4.2. http://www.iq.usp.br/gutz/Curtipot_.html.

(25) Martínez, L.; Andrade, R.; Birgin, E. G.; Martínez, J. M. PACKMOL: a package for building initial configurations for molecular dynamics simulations. *J. Comput. Chem.* **2009**, *30*, 2157−2164.

(26) Iler, R. K. *The Chemistry of Silica: Solubility, Polymerization, Colloid and Surface Properties and Biochemistry of Silica*; John Wiley & Sons, 1979.

(27) van der Spoel, D.; Lindahl, E.; Hess, B. *GROMACS User's Manual*, version 4.6.3; 2013.

(28) Nosé, S. A molecular dynamics method for simulations in the canonical ensemble. *Mol. Phys.* **1984**, *52*, 255−268.

(29) Parrinello, M.; Rahman, A. Polymorphic transitions in single crystals: A new molecular dynamics method. *J. Appl. Phys.* **1981**, *52*, 7182−7190.

(30) Hockney, R. W.; Goel, S. P.; Eastwood, J. W. Quiet high-resolution computer models of a plasma. *J. Comput. Phys.* **1974**, *14*, 148−158.

(31) Berendsen, H. J. C.; Grigera, J. R.; Straatsma, T. P. The missing term in effective pair potentials. *J. Phys. Chem.* **1987**, *91*, 6269−6271.

(32) Nagarajan, R. Self-Assembly of Bola Amphiphiles. *Chem. Eng. Commun.* **1987**, *55*, 251−273.

(33) Jorgensen, W. L.; Maxwell, D. S.; Tirado-Rives, J. Development and Testing of the OPLS All-Atom Force Field on Conformational Energetics and Properties of Organic Liquids. *J. Am. Chem. Soc.* **1996**, *118*, 11225−11236.

(34) Wang, J.; Wolf, R. M.; Caldwell, J. W.; Kollman, P. A.; Case, D. A. Development and testing of a general amber force field. *J. Comput. Chem.* **2004**, *25*, 1157−1174.

(35) Caleman, C.; van Maaren, P. J.; Hong, M.; Hub, J. S.; Costa, L. T.; van der Spoel, D. Force Field Benchmark of Organic Liquids: Density, Enthalpy of Vaporization, Heat Capacities, Surface Tension,

DOI: 10.1021/acs.langmuir.6b01731
Langmuir 2016, 32, 7228−7240

Isothermal Compressibility, Volumetric Expansion Coefficient, and Dielectric Constant. *J. Chem. Theory Comput.* **2012**, *8*, 61−74.
(36) Hess, B.; Bekker, H.; Berendsen, H. J. C.; Fraaije, J. G. E. M. LINCS: A linear constraint solver for molecular simulations. *J. Comput. Chem.* **1997**, *18*, 1463−1472.
(37) Darden, T.; York, D.; Pedersen, L. Particle mesh Ewald: An $N \cdot log(N)$ method for Ewald sums in large systems. *J. Chem. Phys.* **1993**, *98*, 10089−10092.
(38) Darden, T.; Perera, L.; Li, L.; Pedersen, L. New tricks for modelers from the crystallography toolkit: the particle mesh Ewald algorithm and its use in nucleic acid simulations. *Structure* **1999**, *7*, R55−R60.
(39) Hoshen, J.; Kopelman, R. Percolation and cluster distribution. I. Cluster multiple labeling technique and critical concentration algorithm. *Phys. Rev. B* **1976**, *14*, 3438−3445.
(40) Kirkwood, J. G.; Buff, F. P. The Statistical Mechanical Theory of Surface Tension. *J. Chem. Phys.* **1949**, *17*, 338−343.
(41) Irving, J. H.; Kirkwood, J. G. The Statistical Mechanical Theory of Transport Processes. IV. The Equations of Hydrodynamics. *J. Chem. Phys.* **1950**, *18*, 817−829.
(42) Humphrey, W.; Dalke, A.; Schulten, K. VMD: visual molecular dynamics. *J. Mol. Graphics* **1996**, *14*, 33−38. 27−28
(43) Israelachvili, J. N. *Intermolecular and Surface Forces*, 3rd ed.; Academic Press, 2011.
(44) Prince, L. M. A theory of aqueous emulsions I. Negative interfacial tension at the oil/water interface. *J. Colloid Interface Sci.* **1967**, *23*, 165−173.
(45) Chakraborty, P.; Zachariah, M. R. Effective" Negative Surface Tension: A Property of Coated Nanoaerosols Relevant to the Atmosphere. *J. Phys. Chem. A* **2007**, *111*, 5459−5464.
(46) Baoukina, S.; Monticelli, L.; Amrein, M.; Tieleman, D. P. The Molecular Mechanism of Monolayer-Bilayer Transformations of Lung Surfactant from Molecular Dynamics Simulations. *Biophys. J.* **2007**, *93*, 3775−3782.
(47) Marrink, S. J.; de Vries, A. H.; Tieleman, D. P. Lipids on the move: Simulations of membrane pores, domains, stalks and curves. *Biochim. Biophys. Acta, Biomembr.* **2009**, *1788*, 149−168.

DOI: 10.1021/acs.langmuir.6b01731
Langmuir 2016, 32, 7228−7240

Supporting Information:

Molecular simulation study of the early stages of formation of bioinspired mesoporous silica materials

Alessia Centi, and Miguel Jorge*

Department of Chemical and Process Engineering, University of Strathclyde, James Weir Building, 75 Montrose Street, Glasgow G1 1XJ

E-mail: miguel.jorge@strath.ac.uk

Force field parameters

Parameters used to model diamine surfactants, bromide and TMA ions were taken from the OPLS all-atom force field.[1,2] Water molecules were modelled using the SPC/E potential[3] and parameters for both neutral and anionic silica were taken from the work of Jorge et al.[4] (see Table S1 - Table S4).

*To whom correspondence should be addressed

Table S1: Lennard-Jones parameters, point charges and atomic masses.

Site	Mass (a.u.)	q (C)	σ (nm)	ε (kJ mol^{-1})
Ow	15.9994	-0.8476	0.31656	0.65019
Hw	1.0080	0.4238	0.0	0.0
N	14.0067	-0.900	0.330	0.711280
Nc	14.0067	-0.300	0.3250	0.711280
Nt	14.0067	0.000	0.3250	0.711280
Cn	12.0110	0.060	0.350	0.276144
Cnc	12.0110	0.190	0.350	0.276144
C	12.0110	-0.120	0.350	0.2761444
Ct	12.0110	0.130	0.350	0.2761444
Hc	1.0080	0.060	0.250	0.125520
Hn	1.0080	0.360	0.0	0.0
Hnc	1.0080	0.330	0.0	0.0
Hcn	1.0080	0.060	0.250	0.06276
Br	79.9040	-1.0	0.462376	0.376560
SiI	28.0855	1.0801	0.4435	0.39748
OhI	15.9994	-0.7481	0.34618	0.665674
HoI	1.0080	0.3684	0.23541	0.413379
Oc	15.9994	-0.9410	0.34618	0.665674

Table S2: Bond lengths.

Bond	Lenght (nm)
Ow-Hw	0.100
N-Hn	0.101
N-Cn	0.1448
Nc-Hcn	0.101
Nc-Cnc	0.1471
Nt-Ct	0.1471
Cn-Hcn	0.109
Cn-C	0.1529
Cnc-Hc	0.109
Cnc-C	0.1529
C-Hc	0.109
C-C	0.1529
Ct-Hc	0.109
SiI-OhI	0.169
SiI-Oc	0.158
OhI-HoI	0.097

Table S3: Bond angles and harmonic force constants.

Angle	θ_0 (deg)	k_θ k (kJ mol^{-1} rad^{-2})
Hw-Ow-Hw	109.47	—
Hn-N-Hn	106.4	364.845
Hn-N-Cn	109.5	292.880
Hnc-Nc-Hnc	109.5	292.880
Hnc-Nc-Cnc	109.5	292.880
N-Cn-C	109.47	470.281
N-Cn-Hcn	109.5	292.880
Nc-Cnc-C	111.2	669.44
Nc-Cnc-Hcn	109.5	292.800
Nt-Ct-Hc	109.5	292.880
Hcn-Cn-Hcn	107.8	276.144
Hcn-Cn-C	110.7	313.800
Hcn-Cnc-Hcn	107.8	276.144
Hcn-Cnc-C	110.7	313.800
Cn-C-C	112.7	488.273
Cn-C-Hc	110.7	313.800
Cnc-C-C	112.7	488.273
Cnc-C-Hc	110.7	313.800
Ct-Nt-Ct	113.0	418.400
Hc-C-C	110.7	313.800
Hc-C-Hc	107.8	276.144
Hc-Ct-Hc	107.8	276.144
C-C-C	112.7	488.273
SiI-OhI-HoI	109.8	103.46
OhI-SiI-OhI	104.9	232.96
OhI-SiI-Oc	114.2	232.96

Table S4: Dihedral torsion parameters.

Dihedral	C_0 (kJ mol^{-1})	C_1 (kJ mol^{-1})	C_2 (kJ mol^{-1})	C_3 (kJ mol^{-1})	C_4 (kJ mol^{-1})	C_5 (kJ mol^{-1})
Hn-N-Cn-Hcn	0.83680	2.51040	0.0	-3.34720	0.0	0.0
Hn-N-Cn-C	-1.26775	3.02085	1.74473	-3.49782	0.0	0.0
Hnc-Nc-Cnc-Hcn	0.54601	1.63803	0.0	-2.18405	0.0	0.0
Hnc-Nc-Cnc-C	-1.26775	3.02085	1.74473	-3.49782	0.0	0.0
N-Cn-C-Hc	-4.09614	5.08775	2.96645	-3.95806	0.0	0.0
N-Cn-C-C	3.33465	-1.5526	2.82001	-4.60240	0.0	0.0
Nc-Cnc-C-C	5.77183	-2.67148	0.95814	-4.05848	0.0	0.0
Nc-Cnc-C-Hc	0.8033	2.4099	0.0	-3.21331	0.0	0.0
Hcn-Cn-C-Hc	0.62760	1.88280	0.0	-2.51040	0.0	0.0
Hcn-Cn-C-C	0.62760	1.88280	0.0	-2.51040	0.0	0.0
Hcn-Cnc-C-Hc	0.62760	1.88280	0.0	-2.51040	0.0	0.0
Hcn-Cnc-C-C	0.62760	1.88280	0.0	-2.51040	0.0	0.0
Hc-Ct-Nt-Ct	0.63179	1.89535	0.0	-2.52714	0.0	0.0
Cn-C-C-C	2.92880	-1.46440	0.20920	-1.67360	0.0	0.0
Cnc-C-C-C	2.92880	-1.46440	0.20920	-1.67360	0.0	0.0
C-C-C-C	2.92880	-1.46440	0.20920	-1.67360	0.0	0.0
OhI-SiI-OhI-HoI	14.8473	9.1554	-3.6233	2.0686	0.0	0.0
Oc-SiI-OhI-HoI	14.8473	9.1554	-3.6233	2.0686	0.0	0.0

pH curves

Figure S1 and Figure S2 show the pH curves for the reference and the monomeric solution respectively, obtained using the utility CurTiPot.[5] pKa for silicic acid[6] and 1,12-diaminododecane[7] have been added to the utility database which already provides the dissociation constants for several acids and bases. Using the pH tab we calculated the species distribution in the reference system and in the monomeric solution (considering a ratio 2 to 1 of silicic acid to amine) at different pH values (i.e changing the concentration of HCl acid or NaOH base).

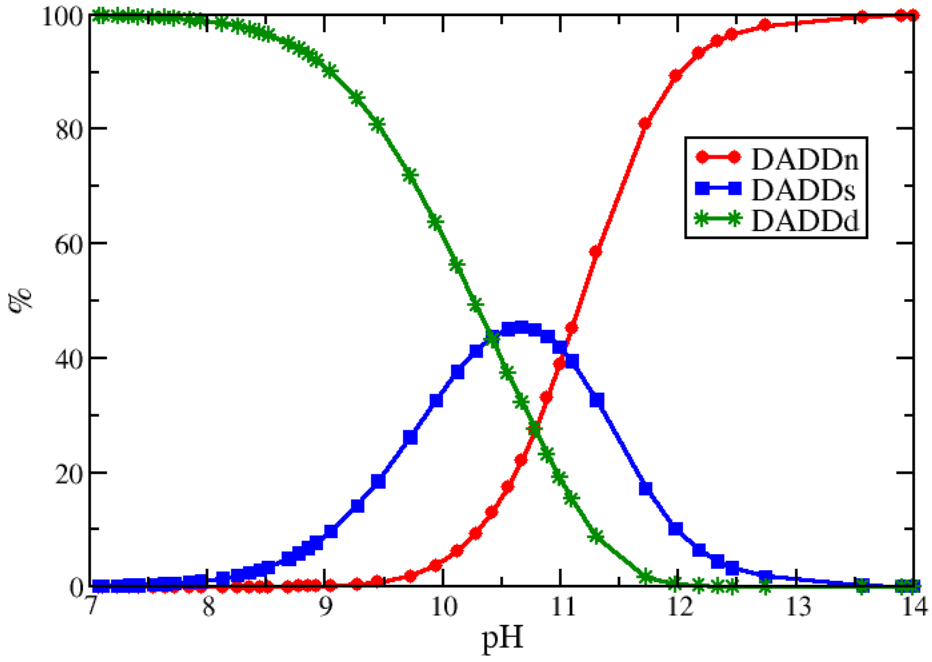

Figure S1: Titration curves for 1,12-diaminododecane in water

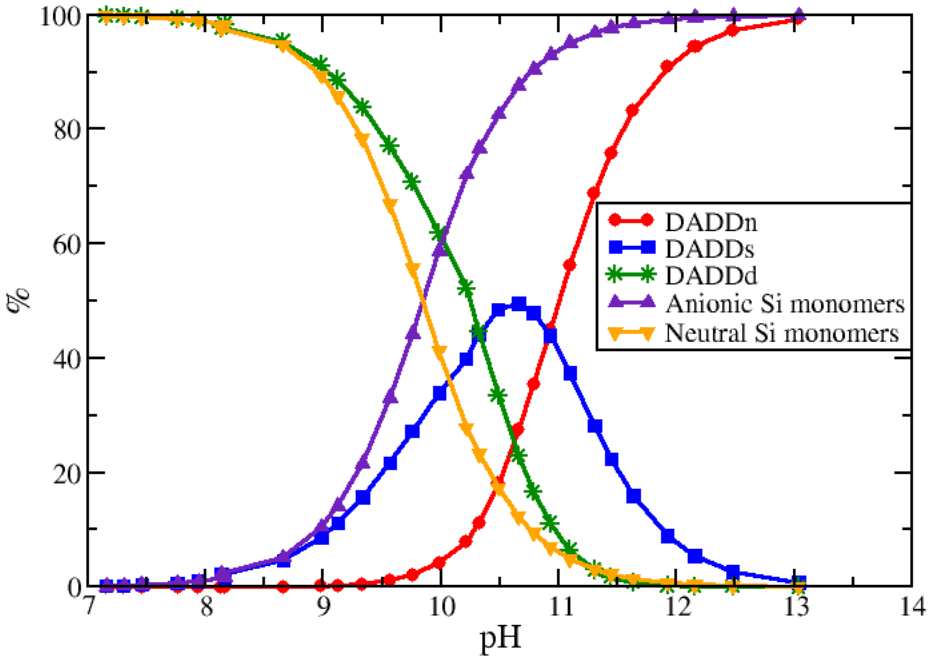

Figure S2: Titration curves for 1,12-diaminododecane with silicic acid in water

Bilayer test

Figure S3 and Figure S4 show the final configuration obtained for the bilayer system and the corresponding density profile (simulation P1-DADDn in Table 1). The initial configuration in this simulation was created using the software Packmol[8] by placing two identical layers, each containing 136 surfactants, separated by two water slabs containing 726 water molecules. The total number of water molecules is the same as that used in the simulation R4-DADDn (see Table 1) whereas the number of surfactants in the layer was chosen considering our results for the reference system R2-DADDn, which produced a complete horizontal layer. Furthermore, we account for the remaining surfactants in R4-DADDn (277 in total) by adding in each water slab three DADDn molecules. The simulation was performed using the same parameters described in Table 1 for 20 ns.

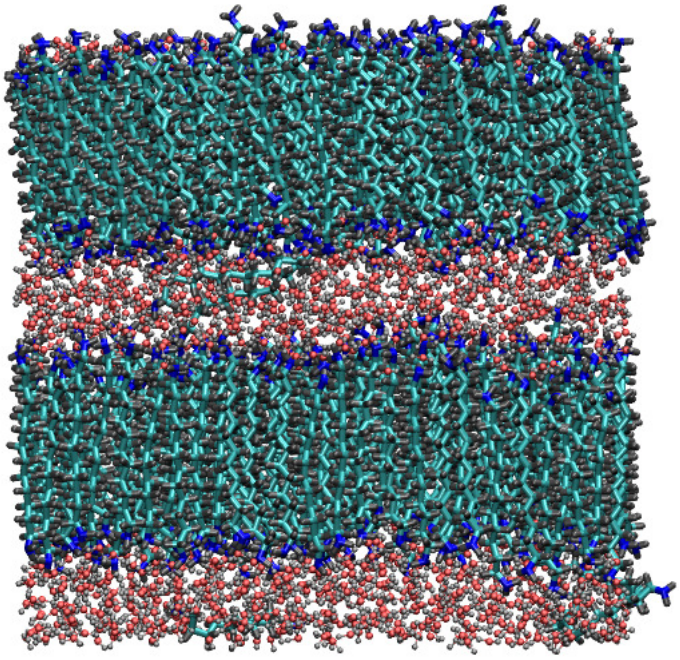

Figure S3: Snapshot of the bilayer system created using Packmol (P1-DADDn). Colour code is the same as in Figure 2.

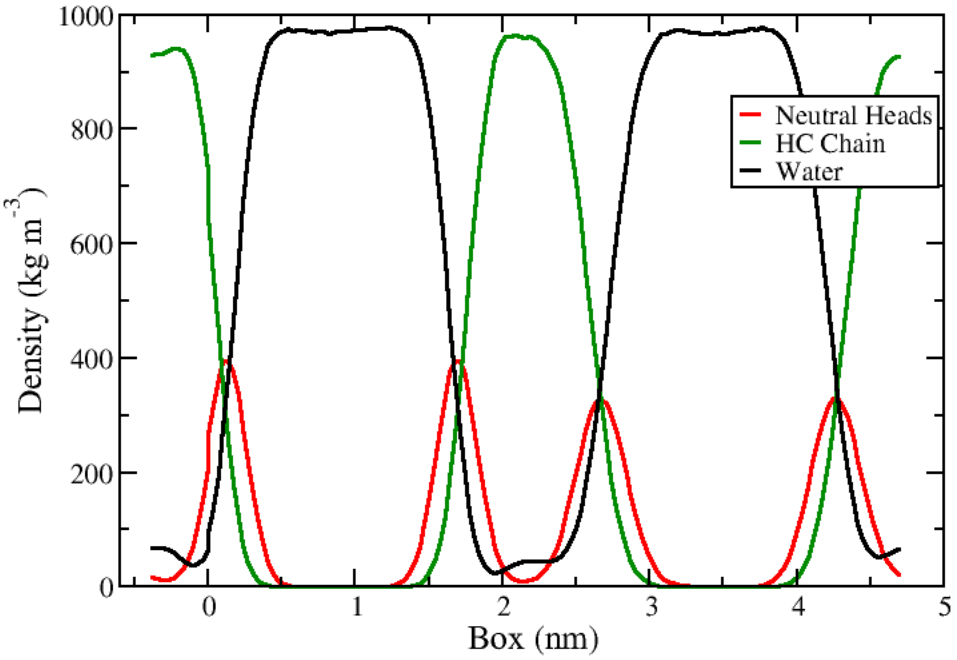

Figure S4: Density profile across the box in the bilayer system. See labels for details.

Cluster counting calculations

Figure S5 shows the evolution of the average cluster size calculated for the neutral system with different concentrations of surfactants.

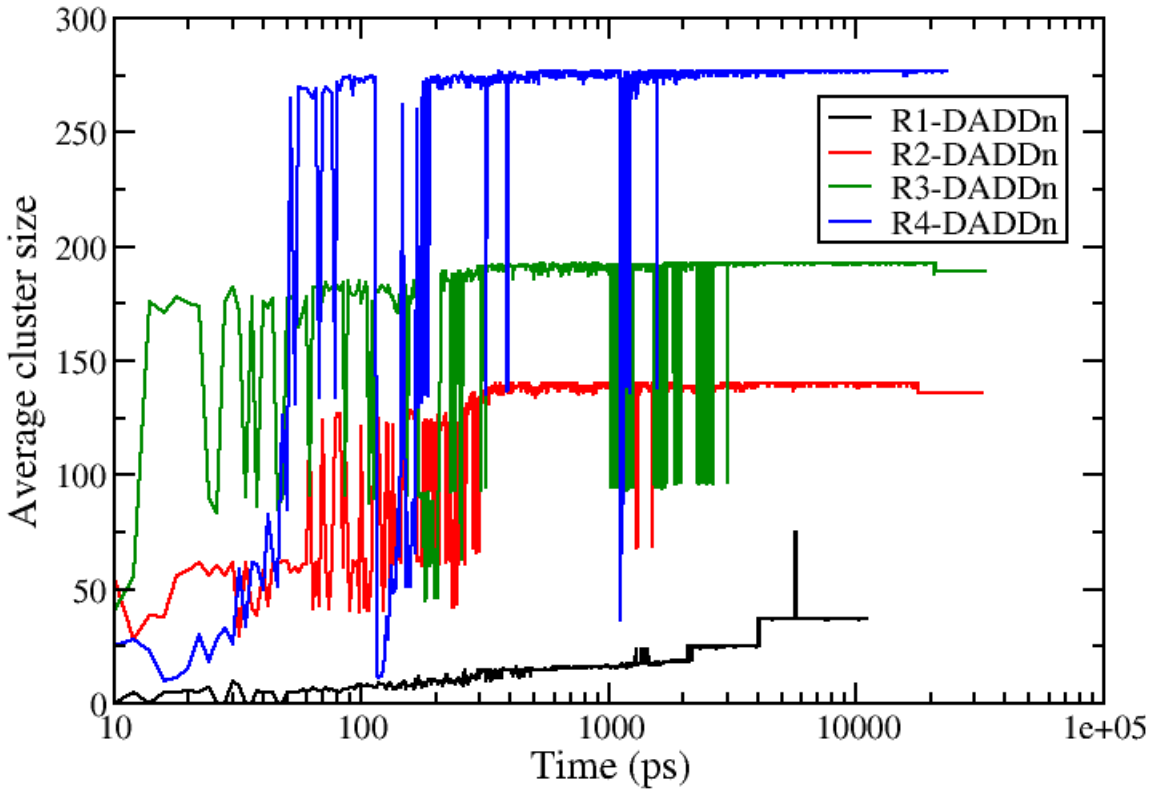

Figure S5: Evolution the average cluster size for simulations with different concentration of neutral surfactant, listed in Table 1.The total number of surfactants is respectively 75 (R1-DADDn), 140 (R2-DADDn), 193 (R3-DADDn), 277 (R4-DADDn). See labels for details.

Figure S6 shows a comparison between the number of clusters and number-average cluster size calculated for the neutral systems containing 140 surfactants: R2-DADDn starting from random initial configurations of surfactants and P2-DADDn starting from a preformed layer.

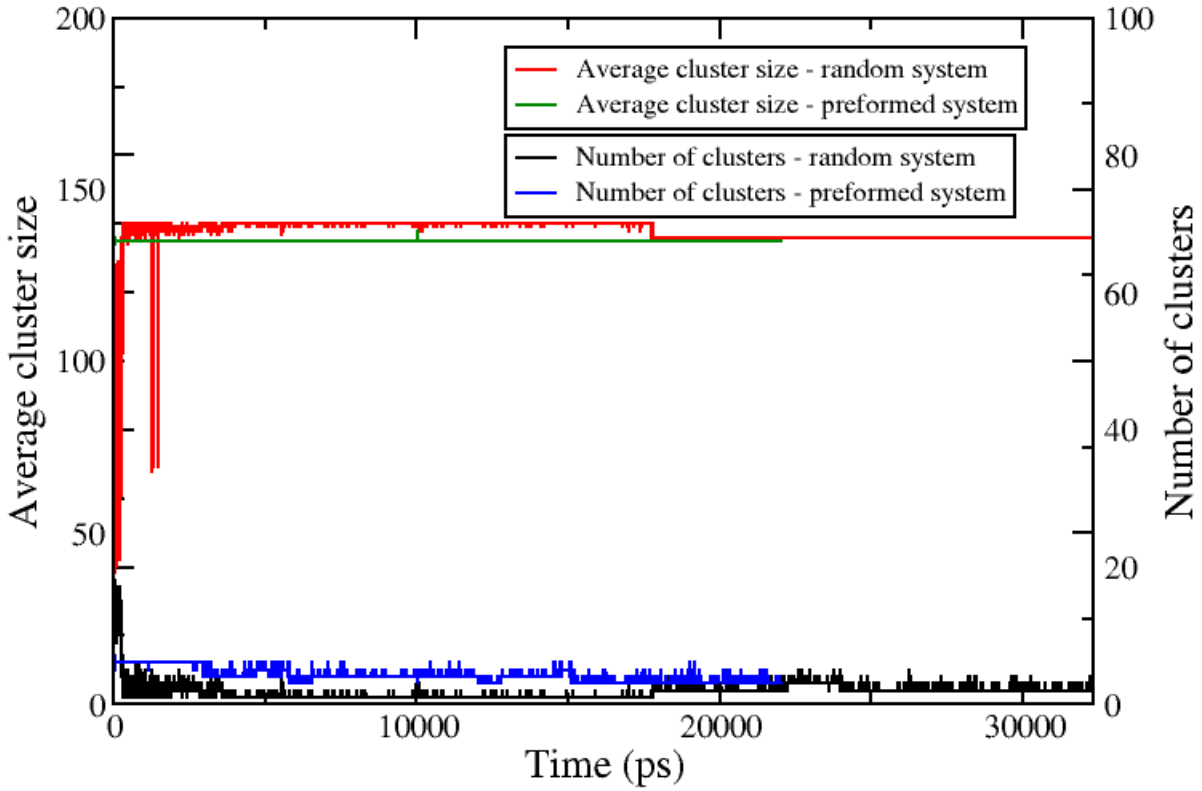

Figure S6: Comparison between simulation results starting from random initial configurations of surfactants (R2-DADDn) and from preformed layer (P2-DADDn). See labels for details.

Figure S7 shows a comparison between number of clusters and number average cluster size obtained for the singly charged system from random and preformed simulations.

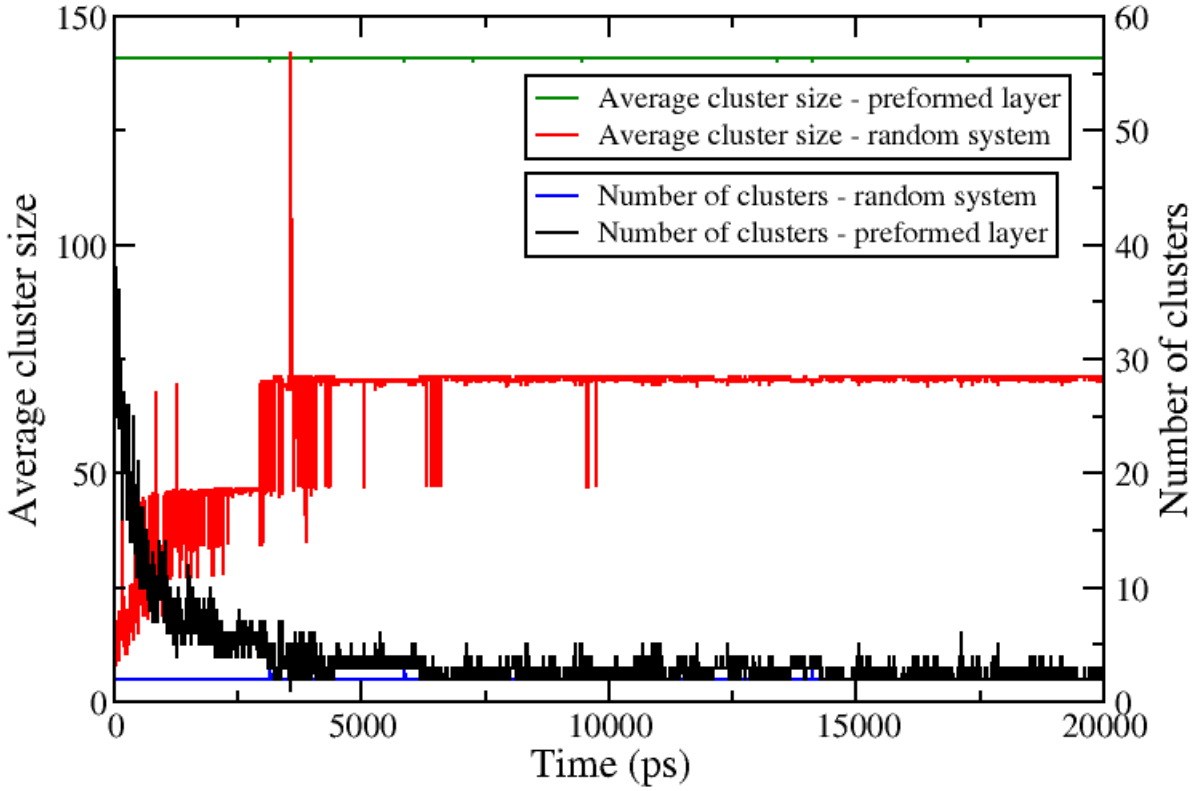

Figure S7: Comparison between simulation results obtained for the singly charged system for simulations starting from random (R5-DADDs) and from a preformed layer (P3-DADDs). Number of clusters: random (red), packmol (black); Number average cluster size: random (dark green), packmol (blue).

Figure S8 compares the average cluster size obtained in the reference solution with DADDd surfactants at different concentrations.

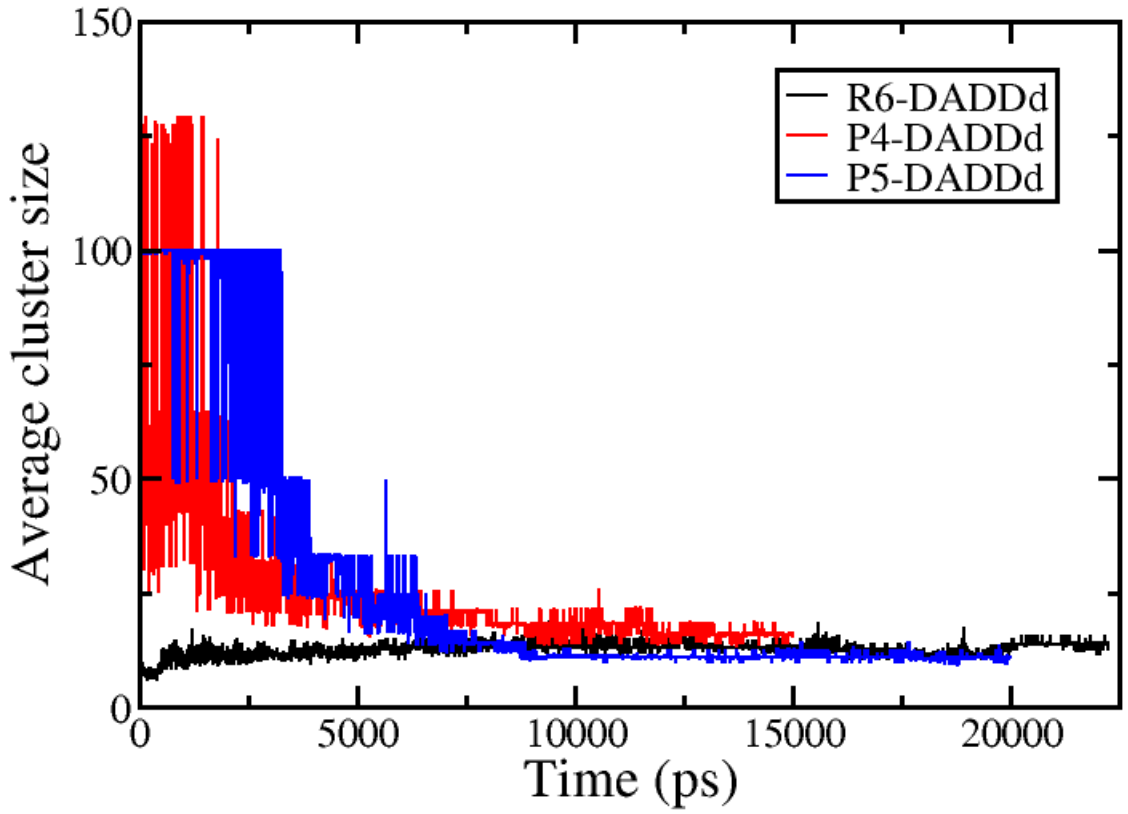

Figure S8: Comparison between average cluster size obtained for the reference solution with DADDd surfactants at different concentrations. R6-DADDd, black; P4-DADDd, red; P5-DADDd, blue.

RDFs comparison

Figure S9 shows a comparison between the radial distribution functions obtained for singly charged systems when starting from preformed layers (dashed lines) and from random initial configurations (solid lines).

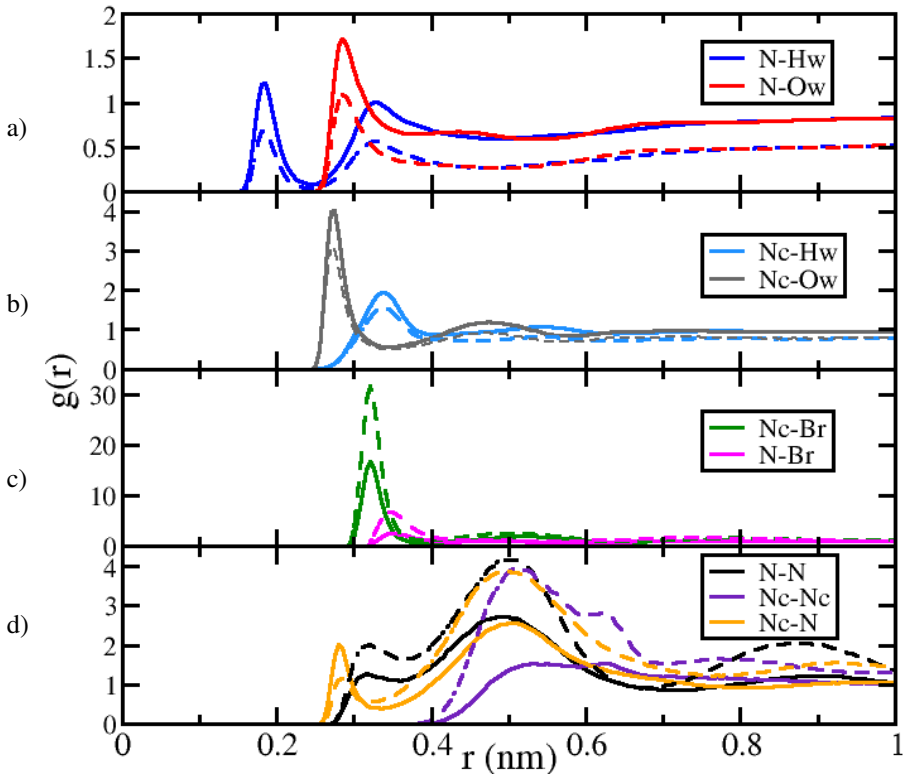

Figure S9: Radial distribution function obtained in P3-DADDs (dashed lines) and R5-DADDs (solid lines): for a) interactions between neutral heads and water, b) interactions between charged heads and water, c) interactions between heads and bromide, d) interactions between neutral and charged heads. See labels for details.

Figure S10 shows a comparison between the radial distribution functions obtained for neutral (solid lines), singly charged (dashed lines) and doubly charged (dotted line) systems starting from random configurations of surfactants.

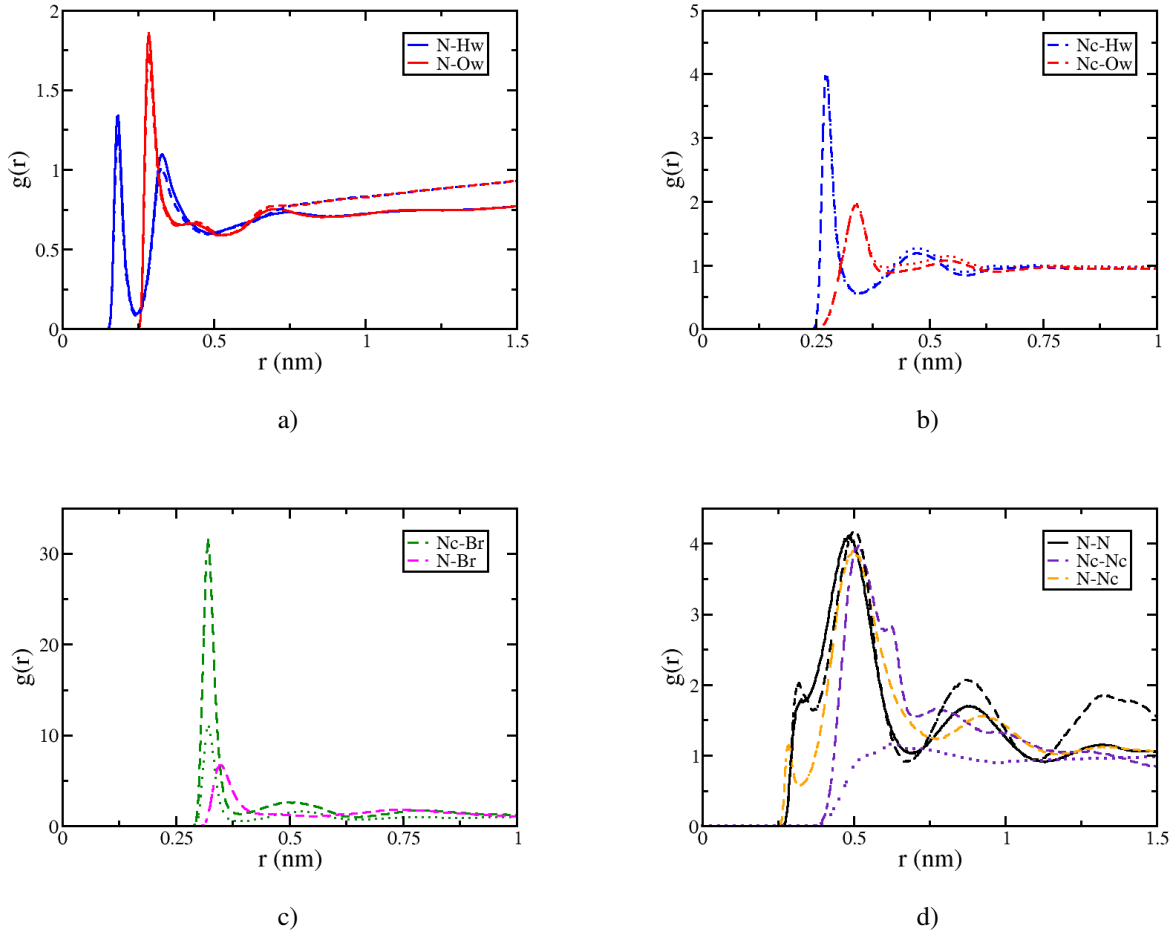

Figure S10: Comparison between radial distribution functions obtained for simulations starting from random configuration of surfactants R2-DADDn (solid lines), R5-DADDs (dashed lines) and R6-DADDd (dotted lines): for a) interactions between neutral heads and water, b) interactions between charged heads and water, c) interactions between heads and bromide, d) interactions between neutral and charged heads. See labels for details.

Figure S11 shows the radial distribution functions for the system P6-DADDn-Si.

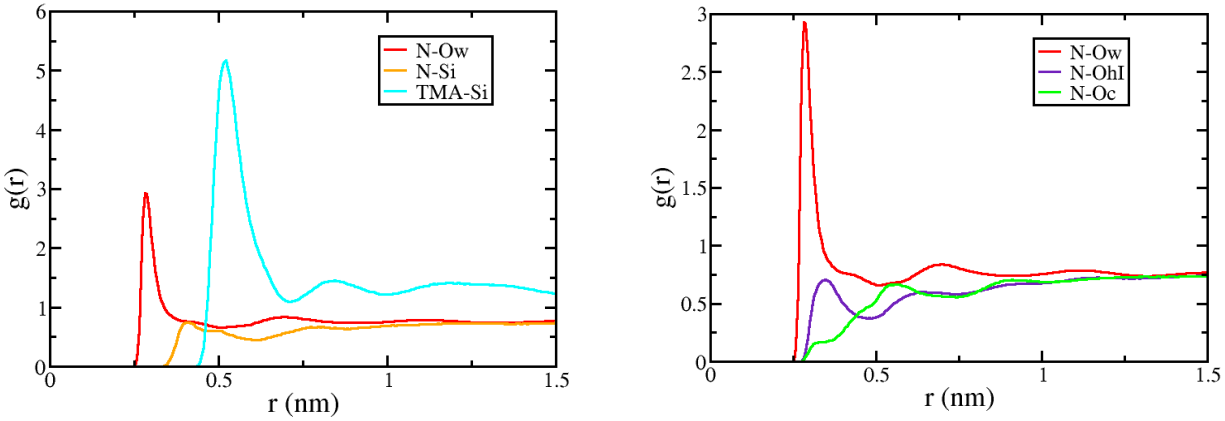

Figure S11: Radial distribution functions for the system P6-DADDn-Si, see labels for details.

Energy calculations

Table S5: Energies of interactions in the reference systems P2-DADDn, P3-DADDs and P4-DADDd. Surfactant and Surfactant-Water energies are normalised by the number of surfactant molecules in each simulation, Surfactant-Bromide energies are normalised by the number of bromide counterions.

Surfactant-Surfactant						
	P2-DADDn		P3-DADDs		P4-DADDd	
Coulombic (kJ/mol)	10.26	0.05	52.76	0.16	78.44	0.69
LJ (kJ/mol)	-68.02	0.10	-62.93	1.93	-28.03	0.12
Total (kJ/mol)	-57.76	0.11	-10.16	1.94	50.41	0.70
Surfactant-Water						
	P2-DADDn		P3-DADDs		P4-DADDd	
Coulombic (kJ/mol)	-95.26	0.12	-132.98	0.99	-258.31	2.23
LJ (kJ/mol)	0.04	0.07	9.40	0.06	2.10	0.18
Total (kJ/mol)	-95.23	0.14	-123.58	0.99	-256.21	2.24
Surfactant-Bromide						
			P3-DADDs		P4-DADDd	
Coulombic (kJ/mol)			-192.73	1.13	-141.68	3.85
LJ (kJ/mol)			14.83	0.14	8.73	0.46
Total (kJ/mol)			-177.89	1.14	-132.96	3.87

Table S6: Energies of interactions in the monomeric systems P6-DADDn, P7-DADDs and P8-DADDd. Surfactant-Surfactant and Surfactant-Water energies are normalised by the number of surfactant molecules in each simulation, Surfactant-Silica energies are normalised by the number of silica monomers.

Surfactant-Surfactant						
	P6-DADDn		P7-DADDs		P8-DADDd	
Coulombic (kJ/mol)	8.79	0.06	64.45	0.94	120.40	0.42
LJ (kJ/mol)	-70.84	0.04	-67.93	0.1	-29.53	0.12
Total (kJ/mol)	-62.05	0.07	-3.48	0.94	90.87	0.43
Surfactant-Water						
	P6-DADDn		P7-DADDs		P8-DADDd	
Coulombic (kJ/mol)	-80.92	0.31	-67.43	1.27	-72.75	0.77
LJ (kJ/mol)	4.59	0.07	4.86	0.11	-4.63	0.42
Total (kJ/mol)	-76.32	0.32	-62.57	1.27	-77.39	0.88
Surfactant-Silica						
	P6-DADDn		P7-DADDs		P8-DADDd	
Coulombic (kJ/mol)	-7.56	0.08	-319.80	2.46	-318.86	0.85
LJ (kJ/mol)	-5.38	0.1	7.02	0.08	-3.48	0.25
Total (kJ/mol)	-12.93	0.13	-312.79	2.47	-322.33	0.88

References

(1) Jorgensen, W. L.; Maxwell, D. S.; Tirado-Rives, J. Development and Testing of the OPLS All-Atom Force Field on Conformational Energetics and Properties of Organic Liquids. *J. Am. Chem. Soc.* **1996**, *118*, 11225–11236.

(2) Wang, J.; Wolf, R. M.; Caldwell, J. W.; Kollman, P. A.; Case, D. A. Development and testing of a general amber force field. *J. Comput. Chem.* **2004**, *25*, 1157–1174.

(3) Berendsen, H. J. C.; Grigera, J. R.; Straatsma, T. P. The missing term in effective pair potentials. *J. Phys. Chem.* **1987**, *91*, 6269–6271.

(4) Jorge, M.; Gomes, J. R. B.; Cordeiro, M. N. D. S.; Seaton, N. A. Molecular Dynamics Simulation of the Early Stages of the Synthesis of Periodic Mesoporous Silica. *J. Phys. Chem. B* **2009**, *113*, 708–718.

(5) Gutz, I. G. R. *CurTiPot. pH and Acid Base Titration Curves: Analysis and Simulation freeware, version 4.2*. `http://www.iq.usp.br/gutz/Curtipot_.html`.

(6) Iler, R. K. *The Chemistry of Silica: Solubility, Polymerization, Colloid and Surface Properties and Biochemistry of Silica*; John Wiley & Sons, 1979.

(7) Ohtaki, H.; Maeda, M. Ionic Equilibria in Mixed Solvents. VIII. Solvent Effects on the Dissociation of Diprotic Acids in Aqueous Methanol Mixtures. *Bull. Chem. Soc. Jpn.* **1973**, *46*, 2052–2056.

(8) Martínez, L.; Andrade, R.; Birgin, E. G.; Martínez, J. M. PACKMOL: a package for building initial configurations for molecular dynamics simulations. *J Comput Chem* **2009**, *30*, 2157–2164.